Heliyon 10 (2024) e24814

Contents lists available at ScienceDirect

Heliyon

journal homepage: www.cell.com/heliyon

Research article

Guanidinium and hydrogen carbonate rosette layers: Distance and degree topological indices, Szeged-type indices, entropies, and NMR spectral patterns

Micheal Arockiaraj [a,*], J. Celin Fiona [a], Jessie Abraham [b], Sandi Klavžar [c,d,e], Krishnan Balasubramanian [f]

[a] Department of Mathematics, Loyola College, Chennai 600034, India
[b] Department of Mathematics, KCG College of Technology, Chennai 600097, India
[c] Faculty of Mathematics and Physics, University of Ljubljana, Slovenia
[d] Institute of Mathematics, Physics and Mechanics, Ljubljana, Slovenia
[e] Faculty of Natural Sciences and Mathematics, University of Maribor, Slovenia
[f] School of Molecular Sciences, Arizona State University, Tempe, AZ 85287-1604, USA

ARTICLE INFO

Keywords:
Supramolecular chemistry
Guanidinium and hydrogen carbonate rosette layer
Distance-degree based topological indices
Szeged and degree-type entropies measures
Proton, ^{13}C, ^{14}N, ^{17}O NMR spectra

ABSTRACT

Supramolecular chemistry explores non-covalent interactions between molecules, and it has facilitated the design of functional materials and understanding of molecular self-assembly processes. We investigate a captivating class of supramolecular structures, the guanidinium and hydrogen carbonate rosette layers. These rosette layers are composed of guanidinium cations and carbonate anions, exhibiting intricate hydrogen-bonding networks that lead to their unique structural properties. Topological and entropy indices unveil the connectivity and complexity of the structures, providing valuable insights for diverse applications. We have developed the cut method technique to deconstruct the guanidinium and hydrogen carbonate rosette layers into smaller components and obtain the distance, Szeged-type and entropy measures. Subsequently, we conducted a comparative analysis between topological indices and entropies which contributes to a deeper understanding of the structural complexity of these intriguing supramolecular systems. We have derived the degree based topological indices and entropies of the underlying rosette layers. Furthermore, our computations reveal several isentropic structures associated with degree and entropy indices. We have employed distance vector sequence-based graph theoretical techniques in conjunction with symmetry-based combinatorial methods to enumerate and construct the various NMR spectral patterns which are demonstrated to contrast the isomers and networks of the rosettes.

1. Introduction

Non-covalent interactions play significant roles in determining the structure, stability, and various mechanisms associated with biological macromolecules, such as protein folding, DNA replication, ligand-receptor binding, and the associated biochemical processes [1–5]. While these interactions are individually weak their cumulative effects can significantly influence the performance and

* Corresponding author.
E-mail address: marockiaraj@gmail.com (M. Arockiaraj).

https://doi.org/10.1016/j.heliyon.2024.e24814
Received 22 October 2023; Received in revised form 3 January 2024; Accepted 15 January 2024

Available online 19 January 2024

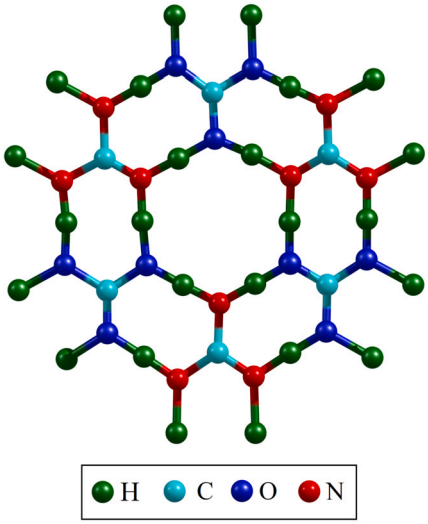

Fig. 1. A unit cell of guanidinium carbonate (GC).

properties of these molecular systems. Hydrogen bonds, in particular, are relatively strong compared to other non-covalent interactions and hence these bonds play a significant role in various biological processes [6–8]. As is well known, oxygen and nitrogen, among other electronegative elements, are often involved in hydrogen bonding due to their ability to form strong partial negative charges as a consequence of their electronegativity. Supramolecular chemistry is the study of assemblies of molecules or ions based on non-covalent interactions such as hydrogen bonding, van der Waals forces, $\pi - \pi$ stacking, and electrostatic and hydrophobic interactions [9–12]. Supramolecular assemblies have a wide range of applications, including drug delivery systems, catalysis, nanotechnology and the development of molecular machines and switches [13–17]. Many biological processes, such as enzyme-substrate interactions, antibody-antigen recognition, and DNA base pairing, are based on supramolecular host-guest complexes [18–22]. One of the most fascinating aspects of supramolecular chemistry is its self-assembly. It explores how molecules with complementary functional groups tend to spontaneously organize themselves into larger, well-defined structures through non-covalent interactions [23–25]. This self-organization feature is harnessed in designing complex architectures and functional materials at the nanoscale. The supramolecular assembly is also observed in nature, for instance, when proteins fold into specific three-dimensional structures through non-covalent interactions, and when lipid bilayers self-assemble to form cell membranes [26,27]. Similarly, DNA molecules can self-assemble into intricate nanostructures through complementary base-pairing interactions [28–30]. In recent years mathematical and artificial intelligence techniques including big data, neural networks, combinatorial, and graph theoretical methods have been shown to have several applications in drug discovery, dynamic reaction networks and so forth [31–34].

The guanidinium ion, denoted as $CH_6N_6^+$, is the cationic form of guanidine ($NH_2C(NH)NH_2$) and hence contains three amino groups (NH_2), which can take part in the H-bonding due to the available lone pair on the nitrogens. Consequently, the guanidinium ion plays a significant role in supramolecular chemistry due to strong intramolecular and intermolecular hydrogen bonding with a variety of molecular species, including anions, polar organic compounds, and water molecules [35,36]. It is often influences biological and chemical processes such as gene therapy, protein and DNA assmeblies, and protein crystallization. Guanidinium carbonate consists of guanidinium cations and carbonate anions held together by ionic bonds. A unit cell of guanidinium carbonate, illustrated in Fig. 1, comprises atoms such as hydrogen, carbon, oxygen, and nitrogen. In contrast, the unit cell of boric acid 2D sheet is relatively similar to guanidinium carbonate, having only six pendant bonds and atoms of hydrogen, boron, and oxygen. Furthermore, the degree based bond partitions of the boric acid 2D structure include the bond classes [37] $(1,3)$, $(2,2)$, $(2,3)$, and $(3,3)$, while guanidinium carbonate has only three classes: $(1,3)$, $(2,3)$, and $(3,3)$. This difference in bond classes results in a high degree of structural symmetry for guanidinium carbonate. Consequently, the topological studies of these two units exhibit differing effects.

A rosette layer arrangement in a material refers to a circular or radial pattern, analogous to the petals of a rose flower. In the context of nanomaterials or molecular assemblies, a rosette layer is comprised of a pattern where certain molecules or molecular groups are arranged in a flower-like configuration [25]. Guanidinium and hydrogen carbonate rosette layers are white or colorless crystalline solids formed by a self-assembly of guanidinium carbonate ribbons by joining through hydrogen bonds to form a several layered sheet like structure with a rosette kind of appearance [38,39]. This assemblage of rosette layers leads to a bitrapezium shaped structure as shown in Fig. 2. Researchers are exploring its potential applications in various fields, ranging from electronics and catalysis to energy storage and biomedical applications [40,41].

Chemical graph theory is a branch of theoretical chemistry and mathematics where chemical compounds are represented as graphs, with atoms as nodes (vertices) and chemical bonds as edges (node connectors). This graph-based representation provides a mathematical framework for analyzing and modeling the various structural and molecular characteristics. Topological indices are numerical values associated with a chemical graph that provide significant information about the graph's underlying connectivity

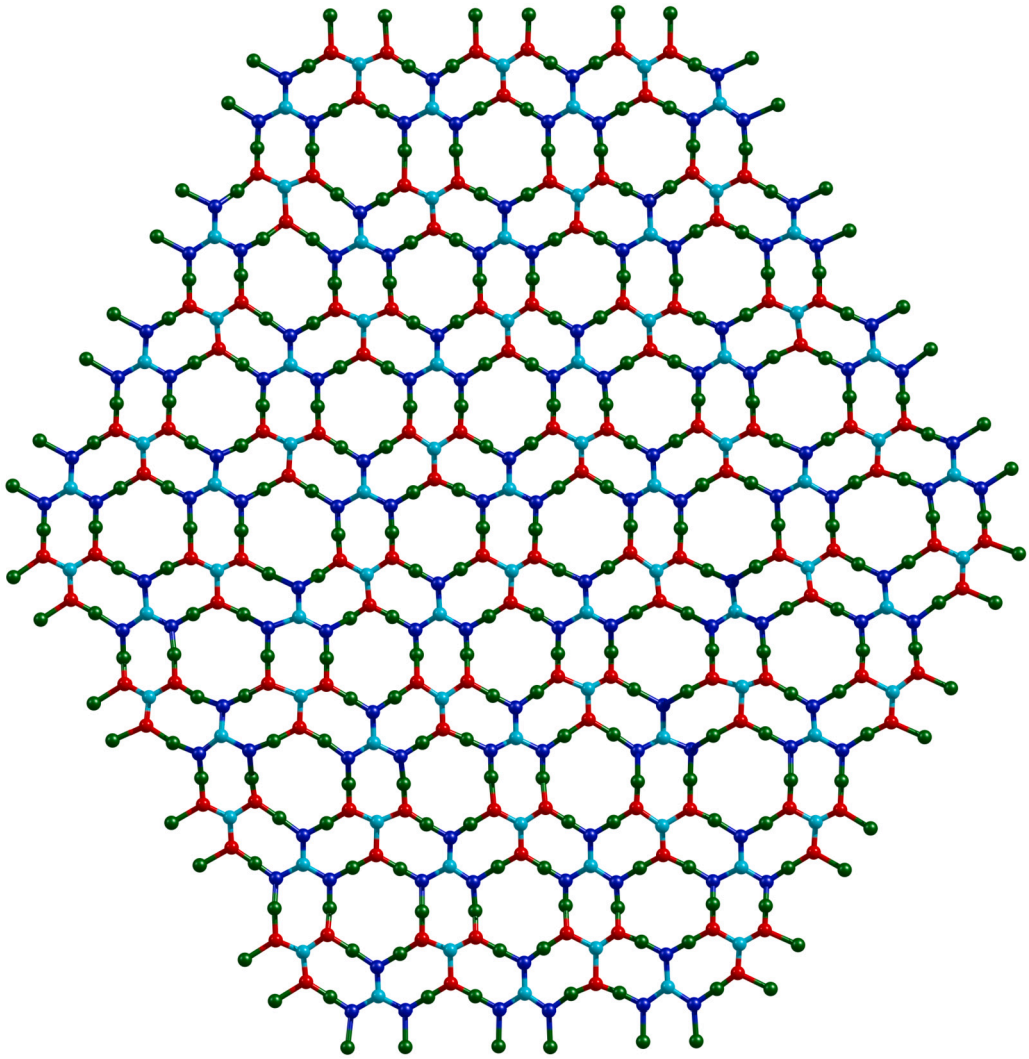

Fig. 2. Bi-trapezium type BT-GC(6, 4).

with the aid of quantitative structure-activity relationship (QSAR) and quantitative structure property relationship (QSPR) studies [42–49]. There are numerous types of topological indices based on factors like distance, atomic-bond connectivity, vertex degree, ring structure, or branching patterns [50,51]. Each index is tailored to capture specific aspects of a molecular structure.

Distance-based topological indices, pioneered by the introduction of the Wiener index, quantify structural characteristics based on the topological distance between atoms in the molecular graph, and these indices have been widely used to describe the physical density or compactness of chemical networks [52]. These indices provide quantitative measures of the structural aspects of molecules and compounds, including their branching patterns. Degree-based topological indices are a class of topological descriptors used particularly in QSAR studies, cheminformatics, and molecular graph theory. These indices are derived based on the number of edges connected to a node, which in turn provides valuable information about the connectivity and branching patterns of atoms for further study [46,53–57]. Information-theoretic entropy, such as Shannon entropy, is a versatile tool that allows researchers to quantify the structural complexity and uncertainty in chemical networks, making it applicable to a wide range of domains within chemistry, biology, and data science [58]. In this study, we discuss the different distance and degree-based indices, along with Shannon entropy and its modified measure of guanidinium and hydrogen carbonate rosette layers, in detail. As various supramolecular assemblies exhibit complex and intricate networks, it becomes necessary to develop network-based mathematical techniques to contrast closely related structures. In this study, it is shown that the title networks exhibit both isentropic and isomeric networks. Thus, it becomes necessary to develop the needed tools to juxtapose their properties, such as spectroscopic properties. We have applied distance degree vector sequence methods in conjunction with symmetry-based combinatorial methods to generate the various NMR spectral patterns of these networks, such as proton NMR spectra, ^{13}C NMR spectra, ^{14}N NMR and ^{17}O NMR spectra of these networks.

2. Computational techniques

To study the distance-based topological indices [59–63] and gain comprehensive insights into the structural traits of guanidinium carbonate (GC), we depict its two-dimensional layout as a simple, connected chemical graph, taking into account the presence of hydrogen atoms, typically disregarded in graph theoretical studies. The graphical representation involves organizing the atoms such as hydrogen, carbon, oxygen, and nitrogen into a distinct assemblage known as the vertex set $V(\mathrm{GC})$, with the interconnecting bonds among these atoms forming the edges denoted by the edge set $E(\mathrm{GC})$. For any vertex $p_1 \in V(\mathrm{GC})$, we define its degree, denoted by $d_{\mathrm{GC}}(p_1)$, as the number of edges that are linked to p_1 and the open neighborhood $N_{\mathrm{GC}}(p_1)$ encompasses the set of vertices that are directly connected to vertex p_1 through edges. Moreover, when considering any two vertices $p_1, p_2 \in V(\mathrm{GC})$, we set $d_{\mathrm{GC}}(p_1, p_2)$ to denote the length of a shortest path between these two vertices, where the length of a path is the number of its edges. The distance $d_{\mathrm{GC}}(p_1, q_1q_2)$ between the vertex p_1 and the edge q_1q_2 is defined as $\min\{d_{\mathrm{GC}}(p_1, q_1), d_{\mathrm{GC}}(p_1, q_2)\}$, while the distance $D_{\mathrm{GC}}(e_1, e_2)$ between two edges $e_1 = p_1p_2$ and $e_2 = q_1q_2$ is $\min\{d_{\mathrm{GC}}(p_1, e_2), d_{\mathrm{GC}}(p_2, e_2)\}$.

We define the neighborhood vertex elements associated with the terminal vertices of $e_1 = p_1p_2$ as follows: $N_{p_1}(e_1|\mathrm{GC}) = \{u \in V(\mathrm{GC}) : d_{\mathrm{GC}}(p_1, u) < d_{\mathrm{GC}}(p_2, u)\}$ and $N_{p_2}(e_1|\mathrm{GC}) = \{u \in V(\mathrm{GC}) : d_{\mathrm{GC}}(p_2, u) < d_{\mathrm{GC}}(p_1, u)\}$. Let $n_{p_1}(e_1|\mathrm{GC})$ and $n_{p_2}(e_1|\mathrm{GC})$ be the number of elements in the sets $N_{p_1}(e_1|\mathrm{GC})$ and $N_{p_2}(e_1|\mathrm{GC})$, respectively. Similarly, we define the neighborhood edge elements associated with the terminal vertices of e_1 as $M_{p_1}(e_1|\mathrm{GC}) = \{uv \in E(\mathrm{GC}) : d_{\mathrm{GC}}(p_1, uv) < d_{\mathrm{GC}}(p_2, uv)\}$ and $M_{p_2}(e_1|\mathrm{GC}) = \{uv \in E(\mathrm{GC}) : d_{\mathrm{GC}}(p_2, uv) < d_{\mathrm{GC}}(p_1, uv)\}$. Further, $m_{p_1}(e_1|\mathrm{GC})$ and $m_{p_2}(e_1|\mathrm{GC})$ stand for the number of elements in the sets $M_{p_1}(e_1|\mathrm{GC})$ and $M_{p_2}(e_1|\mathrm{GC})$, respectively.

Recently, there has been an emergence of topological indices tailored for strength-weighted graphs, which have been extensively explored and discussed in various research papers [37,50,59–61,64,65]. For this purpose, the GC structure was assembled to be the strength-weighted graph $\mathrm{GC}_{sw} = (\mathrm{GC}, (w_v, s_v), s_e)$ where the vertex weight and strength functions are $w_v : V(\mathrm{GC}_{sw}) \to \mathbb{R}_0^+$, $s_v : V(\mathrm{GC}_{sw}) \to \mathbb{R}_0^+$ and the edge strength function is $s_e : E(\mathrm{GC}_{sw}) \to \mathbb{R}_0^+$. The basic graph theoretical terminologies of GC_{sw} are relatively connected to GC structure that are defined as follows: $N_{\mathrm{GC}_{sw}}(p_1) = N_{\mathrm{GC}}(p_1)$, $d_{\mathrm{GC}_{sw}}(p_1, p_2) = d_{\mathrm{GC}}(p_1, p_2)$, $d_{\mathrm{GC}_{sw}}(p_1, q_1q_2) = d_{\mathrm{GC}}(p_1, q_1q_2)$, $D_{\mathrm{GC}_{sw}}(e_1, e_2) = D_{\mathrm{GC}}(e_1, e_2)$, $N_{p_1}(e_1|\mathrm{GC}_{sw}) = N_{p_1}(e_1|\mathrm{GC})$, and $M_{p_1}(e_1|\mathrm{GC}_{sw}) = M_{p_1}(e_1|\mathrm{GC})$. The degree of vertex p_1 in GC_{sw} is defined by the expression $d_{\mathrm{GC}_{sw}}(p_1) = \sum_{x \in N_{\mathrm{GC}_{sw}}(p_1)} s_e(p_1x)$. The cardinality of the closeness measures of the edge $e_1 = p_1p_2$ is calculated by $n_{p_1}(e_1|\mathrm{GC}_{sw}) = \sum_{u \in N_{p_1}(e_1|\mathrm{GC}_{sw})} w_v(u)$, $m_{p_1}(e_1|\mathrm{GC}_{sw}) = \sum_{u \in N_{p_1}(e_1|\mathrm{GC}_{sw})} s_v(u) + \sum_{uv \in M_{p_1}(e_1|\mathrm{GC}_{sw})} s_e(uv)$. The computations of $n_{p_2}(e_1|\mathrm{GC}_{sw})$ and $m_{p_2}(e_1|\mathrm{GC}_{sw})$ are carried out analogously.

We introduce the notation $TI(\mathrm{GC}_{sw})$ to symbolize the distance-based topological indices for the guanidinium and hydrogen carbonate rosette layers. This notation encompasses vertex and edge-based contributions, including indices such as Wiener, Szeged, PI, Schultz, Gutman, and Mostar, which are stated below.

- $W(\mathrm{GC}_{sw}) = \sum_{\{p_1,p_2\} \subseteq V(\mathrm{GC}_{sw})} w_v(p_1) w_v(p_2) d_{\mathrm{GC}_{sw}}(p_1, p_2)$
- $W_e(\mathrm{GC}_{sw}) = \sum_{\{p_1,p_2\} \subseteq V(\mathrm{GC}_{sw})} s_v(p_1) s_v(p_2) d_{\mathrm{GC}_{sw}}(p_1, p_2) + \sum_{\{e_1,e_2\} \subseteq E(\mathrm{GC}_{sw})} s_e(e_1) s_e(e_2) D_{\mathrm{GC}_{sw}}(e_1, e_2) + \sum_{p_1 \in V(\mathrm{GC}_{sw})} \sum_{e_1 \in E(\mathrm{GC}_{sw})} s_v(p_1)\ s_e(e_1)\ d_{\mathrm{GC}_{sw}}(p_1, e_1)$
- $W_{ev}(\mathrm{GC}_{sw}) = \frac{1}{2}\left[\sum_{\{p_1,p_2\} \subseteq V(\mathrm{GC}_{sw})} \{w_v(p_1) s_v(p_2) + w_v(p_2) s_v(p_1)\} d_{\mathrm{GC}_{sw}}(p_1, p_2) + \sum_{p_1 \in V(\mathrm{GC}_{sw})} \sum_{e_1 \in E(\mathrm{GC}_{sw})} w_v(p_1)\ s_e(e_1)\ d_{\mathrm{GC}_{sw}}(p_1, e_1) \right]$
- $S(\mathrm{GC}_{sw}) = \sum_{\{p_1,p_2\} \subseteq V(\mathrm{GC}_{sw})} \left[w_v(p_2)(d_{\mathrm{GC}_{sw}}(p_1) + 2s_v(p_1)) + w_v(p_1)(d_{\mathrm{GC}_{sw}}(p_2) + 2s_v(p_2)) \right] d_{\mathrm{GC}_{sw}}(p_1, p_2)$
- $Gut(\mathrm{GC}_{sw}) = \sum_{\{p_1,p_2\} \subseteq V(\mathrm{GC}_{sw})} (d_{\mathrm{GC}_{sw}}(p_1) + 2s_v(p_1))(d_{\mathrm{GC}_{sw}}(p_2) + 2s_v(p_2)) d_{\mathrm{GC}_{sw}}(p_1, p_2)$
- $Sz_v(\mathrm{GC}_{sw}) = \sum_{e_1 = p_1p_2 \in E(\mathrm{GC}_{sw})} s_e(e_1) n_{p_1}(e_1|\mathrm{GC}_{sw}) n_{p_2}(e_1|\mathrm{GC}_{sw})$
- $Sz_e(\mathrm{GC}_{sw}) = \sum_{e_1 = p_1p_2 \in E(\mathrm{GC}_{sw})} s_e(e_1) m_{p_1}(e_1|\mathrm{GC}_{sw}) m_{p_2}(e_1|\mathrm{GC}_{sw})$
- $PI_v(\mathrm{GC}_{sw}) = \sum_{e_1 = p_1p_2 \in E(\mathrm{GC}_{sw})} s_e(e_1) \left[n_{p_1}(e_1|\mathrm{GC}_{sw}) + n_{p_2}(e_1|\mathrm{GC}_{sw}) \right]$
- $PI_e(\mathrm{GC}_{sw}) = \sum_{e_1 = p_1p_2 \in E(\mathrm{GC}_{sw})} s_e(e_1) \left[m_{p_1}(e_1|\mathrm{GC}_{sw}) + m_{p_2}(e_1|\mathrm{GC}_{sw}) \right]$
- $Mo_v(\mathrm{GC}_{sw}) = \sum_{e_1 = p_1p_2 \in E(\mathrm{GC}_{sw})} s_e(e_1) |n_{p_1}(e_1|\mathrm{GC}_{sw}) - n_{p_2}(e_1|\mathrm{GC}_{sw})|$
- $Mo_e(\mathrm{GC}_{sw}) = \sum_{e_1 = p_1p_2 \in E(\mathrm{GC}_{sw})} s_e(e_1) |m_{p_1}(e_1|\mathrm{GC}_{sw}) - m_{p_2}(e_1|\mathrm{GC}_{sw})|$

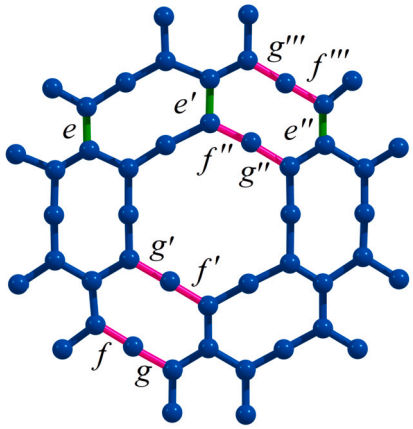

Fig. 3. Two Θ^*-classes of the unit cell of guanidinium carbonate.

The distance-based topological indices of GC structures can be easily deduced from GC_{sw} by considering $w_v = 1, s_v = 0$, and $s_e = 1$. To enhance the efficiency of our computational procedures, we have incorporated the cut method technique [60,61,66,67] for the calculation of topological indices for hydrogen-bonded guanidinium carbonate structures. A subgraph denoted as $H(\mathrm{GC})$ within the graph GC is considered isometric when the distances between vertices p_1 and p_2 in GC is equal to the distances between the same vertices in $H(\mathrm{GC})$. Any isometric subgraph of binary hypercubes is called a partial cube, and in the case of GC structures, it is not a partial cube. Hence, we employ the transitive closure of Djoković-Winkler relation to compute the distance based indices, the technique that was proposed for the first time in [63] for the case of the Wiener index.

The Djoković-Winkler relation Θ is defined by saying that two edges $e_1 = p_1p_2$ and $e_2 = q_1q_2$ of GC are in relation Θ if $d_{\mathrm{GC}}(p_1, q_1) + d_{\mathrm{GC}}(p_2, q_2) \neq d_{\mathrm{GC}}(p_1, q_2) + d_{\mathrm{GC}}(p_2, q_1)$. The transitive closure Θ^* of Θ is a reflexive, symmetric, and transitive relation. Let $\mathscr{B} = \{B_1, B_2, \ldots, B_r\}$ be the partition of the edge set of GC induced by the relation Θ^*, the sets B_i are called the Θ^*-classes. For $1 \leq i \leq r$, the quotient graph GC/B_i has the connected components of $\mathrm{GC} - B_i$ as vertices. Two vertices X and Y of GC/B_i (that is, components of $\mathrm{GC} - B_i$) are adjacent in GC/B_i if there exists an edge $xy \in B_i$ such that vertex x lies in the component X and y lies in the component Y.

Let us apply the above concepts to the unit cell of guanidinium carbonate; at the same time we add that the treatment in general cases is analogous. First, an edge e of an even cycle is in relation Θ to another edge f of the cycle if and only if e and f are opposite edges on the cycle. This property remains valid for each 8-cycle and each 12-cycle of the molecular structures considered in this paper because each of these cycles is an isometric (in fact, even convex) subgraph of the structure. Consider now an arbitrary edge of the unit cell of guanidinium carbonate that lies on the boundary of two 8-cycles, such as the edge e' in Fig. 3. Then e' is in relation Θ to the two respective oposite edges e and e'' on the two 8-cycles in which e' lies. Then $\{e, e', e''\}$ form the Θ^*-class (equivalently, the Θ-class) containing e'. Consequently, the quotient graph of this Θ^*-class is the complete graph on two vertices K_2. Consider next an edge of the unit cell of guanidinium carbonate that simultaneously lies on the boundary of an 8-cycle and a 12-cycle, such as the edge f' from Fig. 3. On the corresponding 8-cycle f' is in relation Θ with the edge f from the figure, while on the 12-cycle, f' is in relation Θ with the edge f''. Further we have $f''\Theta f'''$. We get analogous conclusions for the edges g, g', g'' and g''' from the figure. Moreover, since we can easily infer that f is in relation Θ with g'', we can conclude that $\{f, f', f'', f''', g, g', g'', g'''\}$ form the Θ^*-class containing f'. It follows that the quotient graph of this Θ^*-class is the complete bipartite graph $K_{2,4}$.

Let TI denote a generic topological index such as W, W_e, W_{ev}, S, Gut, Sz_v, Sz_e, PI_v, PI_e, Mo_v, and Mo_e. Then

$$TI(\mathrm{GC}) = \sum_{i=1}^{r} TI(\mathrm{GC}/B_i, (w_v^i, s_v^i), s_e^i) \tag{1}$$

where

- $w_v^i : V(\mathrm{GC}/B_i) \to \mathbb{R}_0^+$, $w_v^i(A) = \sum_{a \in A} w_v(a)$, $\forall\ A \in \mathrm{GC}/B_i$,
- $s_v^i : E(\mathrm{GC}/B_i) \to \mathbb{R}_0^+$, $s_v^i(A) = \sum_{ax \in A} s_e(ax) + \sum_{a \in A} s_v(a)$, $\forall\ A \in \mathrm{GC}/B_i$,
- $s_e^i : E(\mathrm{GC}/B_i) \to \mathbb{R}_0^+$, $s_e^i(AB) = \sum_{\substack{ab \in B_i \\ a \in A,\ b \in B}} s_e(ab)$, $\forall\ AB \in E(\mathrm{GC}/B_i)$.

As observed in the preceding discussion on the Θ classes of the GC structure, we now discuss the special cases of quotient graphs where GC/B_i reduces to either a complete graph on two vertices K_2 or a complete bipartite graph $K_{2,m}$, as shown in Fig. 4(a-b). Subsequently, we derive the associated topological formulas utilized in the calculation of distance based indices for the GC structure.

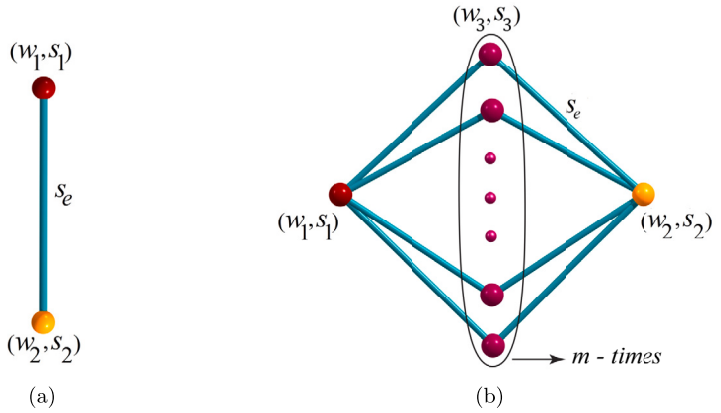

Fig. 4. Special cases of strength weighted graphs (a) K_2 (b) $K_{2,m}$.

Let GC^1_{sw} be the strength weighted graph $\left(K_2,(w_1,s_1),(w_2,s_2),s_e\right)$ as shown in Fig. 4a. Then $W(GC^1_{sw}) = w_1w_2$, $W_e(GC^1_{sw}) = s_1s_2$, $W_{ev}(GC^1_{sw}) = \frac{1}{2}[w_1s_2 + s_1w_2]$, $S(GC^1_{sw}) = w_2(2s_1 + s_e) + w_1(2s_2 + s_e)$, $Gut(GC^1_{sw}) = (2s_1 + s_e)(2s_2 + s_e)$, $Sz_v(GC^1_{sw}) = s_ew_1w_2$, $Sz_e(GC^1_{sw}) = s_es_1s_2$, $PI_v(GC^1_{sw}) = s_e(w_1 + w_2)$, $PI_e(GC^1_{sw}) = s_e(s_1 + s_2)$, $Mo_v(GC^1_{sw}) = s_e|w_1 - w_2|$, and $Mo_e(GC^1_{sw}) = s_e|s_1 - s_2|$.

Let GC^2_{sw} be the strength weighted graph $\left(K_{2,m},(w_1,s_1),(w_2,s_2),(w_3,s_3),s_e\right)$ as shown in Fig. 4b. Then,

- $W(GC^2_{sw}) = w_3^2m^2 + (w_1w_3 + w_2w_3 - w_3^2)m + 2w_1w_2$
- $W_e(GC^2_{sw}) = m(s_1 + s_2)s_3 + 2(s_1s_2) + m(m-1)s_3^2 + m(s_e^2(m-1)) + mse(s_1 + s_2) + 2m(m-1)s_es_3$
- $W_{ev}(GC^2_{sw}) = \frac{1}{2}\left((2s_3w_3 + 2s_ew_3)m^2 + (w_1(s_3 + s_e) + s_1w_3 + s_2w_3 + s_3w_2 - 2s_3w_3 + s_ew_2 - 2s_ew_3)m + 2s_1w_2 + 2s_2w_1\right)$
- $S(GC^2_{sw}) = (2d_{GC_{sw}}(w_3)w_3 + 4s_3w_3)m^2 + (d_{GC_{sw}}(w_1)w_3 + d_{GC_{sw}}(w_2)w_3 + d_{GC_{sw}}(w_3)w_2 - 2d_{GC_{sw}}(w_3)w_3 + 2s_1w_3 + 2s_2w_3 + 2s_3w_2 - 4s_3w_3 + w_1(d_{GC_{sw}}(w_3) + 2s_3))m + 2d_{GC_{sw}}(w_1)w_2 + 4s_1w_2 + w_1(2d_{GC_{sw}}(w_2) + 4s_2)$
- $Gut(GC^2_{sw}) = m((d_{GC_{sw}}(w_3) + 2s_3)((d_{GC_{sw}}(w_1) + s_1) + (d_{GC_{sw}}(w_2) + 2s_2))) + 2((d_{GC_{sw}}(w_1) + 2s_1)(d_{GC_{sw}}(w_2) + 2s_2)) + m(m-1)(d_{GC_{sw}}(w_3) + 2s_3)^2$
- $Sz_v(GC^2_{sw}) = mse\left((w_1w_3 + w_2w_3 + 2w_3^2)m - 2w_3^2 + 2w_1w_2\right)$
- $Sz_e(GC^2_{sw}) = ms_e\left((s_1(s_3 + s_e) + s_2s_3 + s_2s_e + 4s_3s_e + 2s_3^2 + 2s_e^2)m - 2s_3^2 - 4s_3s_e - 2s_e^2 + 2s_1s_2\right)$
- $PI_v(GC^2_{sw}) = 2ms_e\left(w_1 + w_2 + mw_3\right)$
- $PI_e(GC^2_{sw}) = 2ms_e\left(s_1 + s_2 + (s_3 + s_e)m\right)$
- $Mo_v(GC^2_{sw}) = ms_e\left(|w_1 - w_2 - 2w_3 + mw_3| + |w_2 - w_1 - 2w_3 + mw_3|\right)$
- $Mo_e(GC^2_{sw}) = ms_e\left(|s_1 - s_2 - s_3 - s_e + (s_3 + s_e)(m-1)| + |s_2 - s_1 - s_3 - s_e + (s_3 + s_e)(m-1)|\right)$

3. Results and discussion

We examine the various distance based topological and entropy indices for the guanidinium and hydrogen carbonate rosette layers, as they add a unique platform for understanding self-assembly processes and also provide a powerful toolbox for engineering complex structures and unlocking innovative solutions to real-world challenges. The arrangement of GC units in varied ways give rise to different structural pattern of guanidinium carbonate layers in which bi-trapezium shaped structures comprising of large number of GC units. We denote such structure by BT-GC(m,h), where the base layer of trapezium consists of m units in linear pattern and the non-parallel sides with h units such that $m \geq 2$ and $h \leq m$. Fig. 2 shows the guanidinium carbonate rosette layers BT-GC(m,h). The special case of bi-trapezium configuration is deduced by fixing suitable values for m and h [25,38,39]. The linear chain of guanidinium carbonate is obtained by setting $h = 1$ and denoted by L-GC(m). The hexagonal and parallelogram shaped GC layers are obtained by setting $m = 2h - 1$ and $m = h$ respectively which are denoted by H-GC(h) and P-GC(h). These three structures−linear, hexagonal and parallelogram shaped arrangements are shown in Fig. 5(a-c). From the structural pattern of BT-GC(m,h), we have the number of vertices and edges as $28hm - 14h^2 + 30h + 2m + 2$ and $36hm - 18h^2 + 36h$ respectively.

3.1. Distance based topological indices

In this section, we provide the detailed formulations of distance-based topological indices of BT-GC(m,h) in two different cases by splitting the range of h.

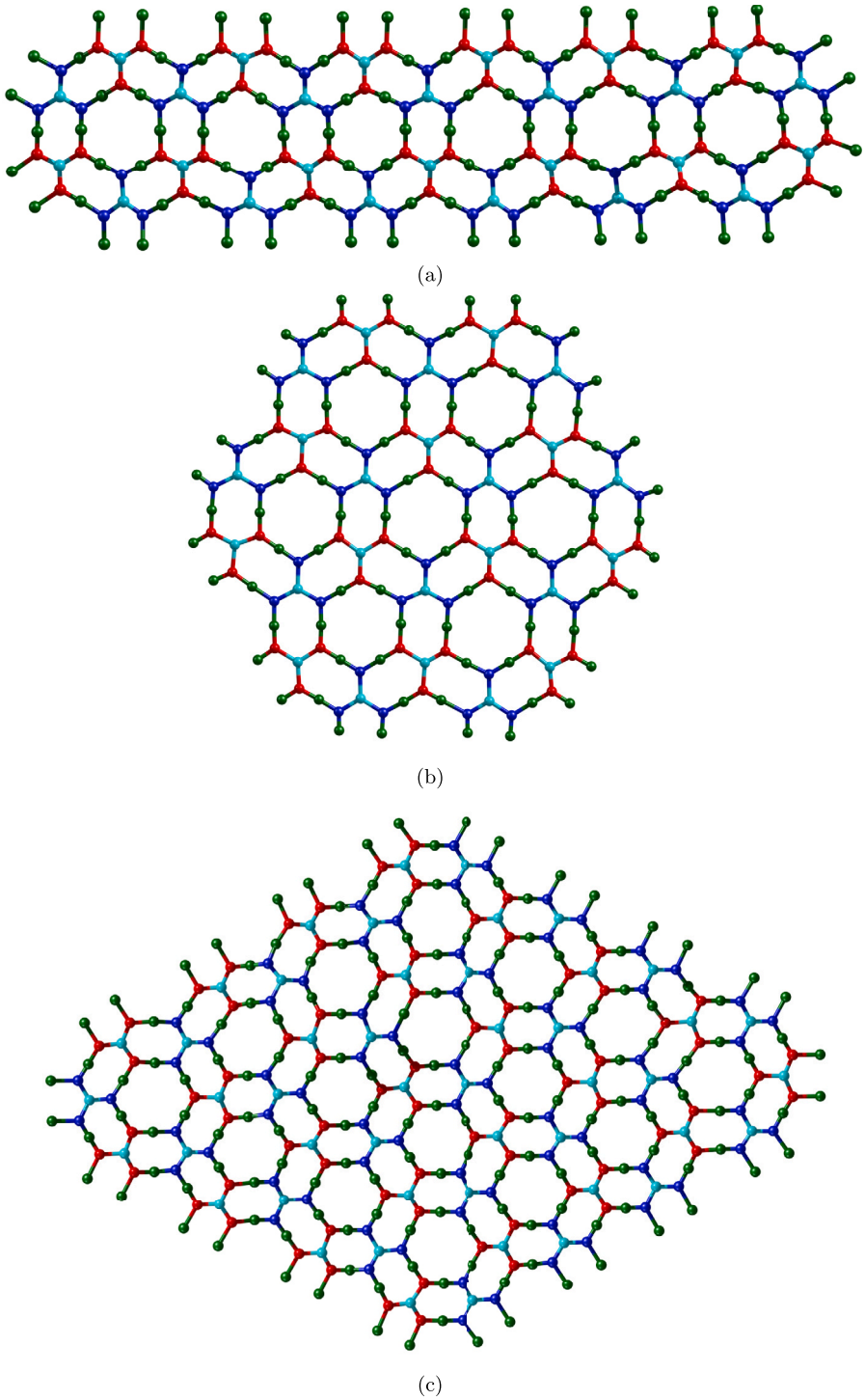

Fig. 5. Special cases of BT-GC(m, h) carbonate rossette (a) Linear chain L-GC(6) (b) Hexagonal layers H-GC(2) (c) Parallelogram layers P-GC(4).

Theorem 1. *Let* BT-GC *be the bi-trapezium type of guanidinium and hydrogen carbonate rosette layers* BT-GC(m, h)*, where* $h \leq \lceil \frac{m}{2} \rceil$*. Then,*

1. $W(\text{BT-GC}) = \frac{2}{5}((1960h^2 + 280h + 10)m^3 - (980h^3 - 6510h^2 - 790h - 40)m^2 - (2100h^3 - 490h^4 - 7250h^2 - 560h - 40)m - 686h^5 + 315h^4 - 1190h^3 + 2810h^2 + 76h + 10)$,

2. $W_e(\text{BT-GC}) = \frac{2}{5}(3240h^2m^3 - (1620h^3 - 8100h^2 + 200h + 10)m^2 + (810h^4 - 1620h^3 + 6555h^2 - 410h - 15)m - 1134h^5 + 405h^4 - 75h^3 + 1680h^2 - 146h - 5)$,
3. $W_{ev}(\text{BT-GC}) = \frac{1}{5}h((5040h + 360)m^3 - (2520h^2 - 14670h - 700)m^2 - (3960h^2 - 1260h^3 - 14280h - 80)m - 1764h^4 + 720h^3 - 1500h^2 + 4770h - 171)$,
4. $S(\text{BT-GC}) = \frac{4}{5}h((5040h + 360)m^3 - (2520h^2 - 15930h - 790)m^2 + (1260h^3 - 5220h^2 + 16845h + 260)m - 1764h^4 + 1035h^3 - 2805h^2 + 6075h - 81)$,
5. $Gut(\text{BT-GC}) = \frac{2}{5}(12960h^2m^3 - (6480h^3 - 38880h^2 + 860h + 20)m^2 + (3240h^4 - 12960h^3 + 39000h^2 - 1800h - 30)m - 4536h^5 + 3240h^4 - 6600h^3 + 13080h^2 - 709h - 10)$,
6. $Sz_v(\text{BT-GC}) = \frac{2}{5}h((11760h^2 + 1960h - 720)m^3 - (17640h^3 - 35560h^2 - 8280h + 2020)m^2 + (8820h^4 - 37310h^3 + 33900h^2 + 11350h - 1780)m - 1470h^5 + 9646h^4 - 20365h^3 + 9430h^2 + 5250h - 426)$,
7. $Sz_e(\text{BT-GC}) = 2((3888h^3 - 216h^2 - 88h)m^3 - (5832h^4 - 11124h^3 + 336h^2 + 256h + 4)m^2 - (10692h^4 - 2916h^5 - 10692h^3 + 54h^2 + 220h + 6)m - 486h^6 + 2592h^5 - 5395h^4 + 3459h^3 + 140h^2 - 46h - 2)$,
8. $PI_v(\text{BT-GC}) = 36h(h - 2m - 2)(7h^2 - m - 14hm - 15h - 1)$,
9. $PI_e(\text{BT-GC}) = 2((648h^2 - 12h + 4)m^2 - (648h^3 - 1260h^2 + 32h - 6)m + 162h^4 - 612h^3 + 624h^2 - 25h + 2)$,
10. $Mo_v(\text{BT-GC}) = 2((252h^2 + 12h + 8)m^2 + (504h^2 - 252h^3 - 6h + 8)m + 74(-1)^m h - 98h - 579h^2 + 628h^3 - 161h^4 + 844(-1)^m h^2 - 880(-1)^m h^3 + 224(-1)^m h^4)$,
11. $Mo_e(\text{BT-GC}) = 2((324h^2 + 4)m^2 + (648h^2 - 324h^3 - 28h + 2)m + 8(-1)^m h - 38h - 846h^2 + 828h^3 - 207h^4 + 1172(-1)^m h^2 - 1152(-1)^m h^3 + 288(-1)^m h^4 - 2)$.

Proof. Due to the symmetry of BT-GC, we consider only the bottom half of vertical bonds from south to north directions. In the bottom trapezium, we see that there are h number of zigzag benzene layers and two consecutive layers linked by bridging back-to-back bonds. For $1 \le j \le h$, let VZ_j be the Θ-class consisting of vertical bonds of j^{th} zigzag layer from south direction. Then the quotient graph BT-GC/VZ_j is a strength weighted graph K_2 with parameters $\big(\text{BT-GC}/VZ_j, (14jm - 14hj + 7j^2 + 9j - 6m + 6h - 5, 18jm - 18hj + 9j^2 + 8j - 10m + 10h - 7), (14hj - 14jm + 28hm - 7j^2 - 14h^2 - 9j + 24h + 8m + 7, 18hj - 18jm + 36hm - 9j^2 - 18h^2 - 10j + 8m + 28h + 6), 1\big)$.

For $1 \le j \le h-1$, let VB_j be the Θ^*-class consisting of binding bonds between j^{th} and $(j+1)^{th}$ zigzag layers. Then BT-GC/VB_j is a strength weighted graph $K_{2,2(m-h+j+1)}$ with parameters $\big(\text{BT-GC}/VB_j, (14jm - 14hj + 7j^2 + 15j, 18jm - 18hj + 9j^2 + 16j - 2m + 2h - 2), (14hj - 14jm + 28hm - 7j^2 - 14h^2 - 17j + 32h, 18hj - 18jm + 36hm - 9j^2 - 18h^2 - 20j + 38h - 2m - 2), (1,0), 1\big)$.

Similarly, we extend our analysis to the acute edge classes and again due to the symmetry of BT-GC structure, we consider only the first h zigzag benzene layers with vertical bonds from north-west to south-east direction. For $1 \le j \le h$, let AZ_j be the Θ-class consisting of vertical bonds of j^{th} layer from north-west direction. Then the quotient graph BT-GC/AZ_j is a strength weighted graph K_2 with parameters $\big(\text{BT-GC}/AZ_j, (14hj + 7j^2 - 5j - 6h + 1, 18hj + 9j^2 - 10j - 10h + 3), (28hm - 14hj - 7j^2 - 14h^2 + 5j + 36h + 2m + 1, 36hm - 18hj - 9j^2 - 18h^2 + 8j + 44h - 2), 1\big)$.

For $1 \le j \le h-1$, let AB_j be the Θ^*-class, consisting of binding bonds between j^{th} and $(j+1)^{th}$ zigzag layers. Hence BT-GC/AB_j is a strength weighted graph of $K_{2,2(h+j)}$ with parameters $\big(\text{BT-GC}/AB_j, (14hj + 7j^2 + j, 18hj + 9j^2 - 2j - 2h), (28hm - 14hj - 14h^2 - 7j^2 - 3j + 28h + 2m + 2, 36hm - 18hj - 18h^2 - 9j^2 - 2j + 34h), (1,0), 1\big)$.

After covering Θ-class AZ_h, there are $m - 2h + 1$ number of zigzag benzene layers of equal size. For $1 \le j \le m - 2h + 1$, let AMZ_j be the Θ-class consisting of vertical bonds of zigzag layers. The quotient graph BT-GC/AMZ_j is a strength weighted graph K_2 with parameters $\big(\text{BT-GC}/AMZ_j, (28hj + 21h^2 - 11h + 2j - 1, 36hj + 27h^2 - 20h), (28hm - 28hj - 35h^2 + 41h - 2j + 2m + 3, 36hm - 36hj - 45h^2 + 52h), 1\big)$.

For $1 \le j \le m - 2h + 2$, let AMB_j be the Θ^*-class with binding bonds between zigzag benzene layers starting from AB_{h-1}. Then BT-GC/AMB_j is a strength weighted graph $K_{2,4h}$ with parameters $\big(\text{BT-GC}/AMB_j, (28hj + 21h^2 + 2j - 27h - 2, 36hj + 27h^2 - 40h), (28hm - 28hj - 35h^2 + 53h - 2j + 2m + 4, 36hm - 36hj - 45h^2 + 68h), (1,0), 1\big)$.

To end with, we have $4(h + m + 1)$ peripheral pendant Θ-class, namely PP_j, $1 \le j \le 4(h + m + 1)$ with quotient graph of K_2, with parameters $\big(\text{BT-GC}/PP_j, (1,0), (28hm - 14h^2 + 30h + 2m + 1, 36hm - 18h^2 + 36h - 1), 1\big)$.

With the above discussed structural information based on Θ^*-parameters of BT-GC(m,h), we can calculate the distance-based topological indices. □

Theorem 2. *Let* BT-GC *be the bi-trapezium type of guanidinium and hydrogen carbonate rosette layers* BT-GC(m,h)*, where* $h > \lceil \frac{m}{2} \rceil$*. Then,*

1. $W(\text{BT-GC}) = \frac{2}{5}((490h - 245)m^4 - 49m^5 + (2240h - 495)m^3 + (2940h^3 + 630h^2 + 3820h - 495)m^2 + (5740h^3 - 3430h^4 + 1190h^2 + 2700h - 226)m + 882h^5 - 3605h^4 + 2850h^3 + 670h^2 + 608h - 30)$,

2. $W_e(\text{BT-GC}) = \frac{2}{15}((2430h-1215)m^4 - 243m^5 + (9720h-2500)m^3 + (14580h^3 - 4860h^2 + 14400h - 2670)m^2 + (34020h^3 - 17010h^4 - 10335h^2 + 9330h - 1352)m + 4374h^5 - 18225h^4 + 19775h^3 - 5520h^2 + 2176h - 210)$,
3. $W_{ev}(\text{BT-GC}) = \frac{1}{15}((3780h - 1890)m^4 - 378m^5 + (16200h - 3880)m^3 + (22680h^3 - 1350h^2 + 25380h - 4080)m^2 + (-26460h^4 + 48600h^3 - 3720h^2 + 16560h - 2012)m + 6804h^5 - 28080h^4 + 26540h^3 - 2010h^2 + 3511h - 300)$,
4. $S(\text{BT-GC}) = \frac{4}{15}((3780h-1890)m^4 - 378m^5 + (16200h-3880)m^3 + (22680h^3 + 2430h^2 + 25650h - 4080)m^2 + (44820h^3 - 26460h^4 + 3975h^2 + 17100h - 2012)m + 6804h^5 - 27135h^4 + 22625h^3 + 1905h^2 + 3781h - 300)$,
5. $Gut(\text{BT-GC}) = \frac{2}{15}((9720h - 4860)m^4 - 972m^5 + (38880h - 9940)m^3 + (58320h^3 + 57060h - 10440)m^2 + (116640h^3 - 68040h^4 - 2280h^2 + 36120h - 5168)m + 17496h^5 - 68040h^4 + 59720h^3 - 2280h^2 + 8029h - 780)$,
6. $Sz_v(\text{BT-GC}) = \frac{2}{5}(14m^5 - (140h+60)m^4 - (760h - 11760h^3 - 2520h^2 + 430)m^3 - (17640h^4 - 34440h^3 - 9960h^2 + 1000h + 700)m^2 - (36190h^4 - 8820h^5 - 29580h^3 - 12430h^2 + 180h + 384)m - 1470h^6 + 9198h^5 - 17165h^4 + 6630h^3 + 4850h^2 + 182h - 40)$,
7. $Sz_e(\text{BT-GC}) = \frac{2}{3}((216h - 138)m^4 - (2052h^2 - 11664h^3 - 1152h + 560)m^3 - (17496h^4 - 36612h^3 + 5220h^2 - 2124h + 768)m^2 - (35100h^4 - 8748h^5 - 36348h^3 + 4200h^2 - 1740h + 394)m - 1458h^6 + 8640h^5 - 17001h^4 + 11365h^3 - 1194h^2 + 554h - 48)$,
8. $PI_v(\text{BT-GC}) = 36h(h-2m-2)(7h^2 - m - 14hm - 15h - 1)$,
9. $PI_e(\text{BT-GC}) = 2(4m^3 + (648h^2 - 36h + 16)m^2 + (1308h^2 - 648h^3 - 80h + 16)m + 162h^4 - 644h^3 + 672h^2 - 45h + 4)$,
10. $Mo_v(\text{BT-GC}) = 2(2m^3 + (252h^2 + 3(-1)^m + 3)m^2 + (528h^2 - 252h^3 - 30h + 11(-1)^m - 15)m + 63h^4 - 268h^3 + 321h^2 - 32h + 8(-1)^m - 16)$,
11. $Mo_e(\text{BT-GC}) = 2((324h^2 + 5(-1)^m - 11)m^2 + (648h^2 - 324h^3 - 28h + 14(-1)^m - 32)m + 81h^4 - 324h^3 + 366h^2 - 30h + 9(-1)^m - 21)$.

Proof. To compute the calculation of topological expressions, we use the proof of the case $h \leq \lceil \frac{m}{2} \rceil$ with the following minor modifications.

- The range of the classes $\{ AZ_j : 1 \leq j \leq h \}$ and $\{ AB_j : 1 \leq j \leq h-1 \}$ are changed into $\{ AZ_j : 1 \leq j \leq m-h+1 \}$ and $\{ AB_j : 1 \leq j \leq m-h \}$ respectively.
- The range of the classes $\{ AMZ_j : 1 \leq j \leq m-2h+1 \}$ into $\{ AMZ_j : 1 \leq j \leq 2h-m-1 \}$ with graph theoretical parameters $\big(\text{BT-GC}/AMZ_j, (14jm + 7m^2 - 7h^2 + 9m - h + 16j + 1, 18jm + 9m^2 - 9h^2 + 8m + 18j - 1), (28hm - 14jm - 7h^2 - 7m^2 - 7m + 31h - 16j + 1, 36hm - 18jm - 9h^2 - 9m^2 - 10m + 36h - 18j - 1), 1\big)$.
- The range of the classes $\{ AMB_j : 1 \leq j \leq m-2h+2 \}$ into $\{ AMB_j : 1 \leq j \leq 2h-m \}$ with graph theoretical parameters $\big(\text{BT-GC}/AMB_j, (14jm + 7m^2 - 7h^2 + m - h + 16j - 8, 18jm + 9m^2 - 9h^2 - 2m + 18j - 11), (28hm - 14jm - 7h^2 - 7m^2 - m + 31h - 16j + 8, 36hm - 18jm - 9h^2 - 9m^2 - 2m + 36h - 18j + 7), (1,0), 1\big)$. □

In addition, we would like to mention that the above derived expressions hold for special cases of bi-trapezium GC(m,h) rosette layers, including linear, hexagonal, and parallelogram types of GC rosette layers. The numerical values of the computed indices are given for parallelogram type GC rosette layers in Table 1.

Table 1
Szeged-type indices of P-GC(h).

TI \ h	1	2	3	4	5	6	7	8	9	10
Sz_v	21690	364152	2288114	9123360	27799530	70800296	158540898	322169040	606789146	1075109976
Sz_e	22356	447264	3029472	12612896	39545468	102793856	233758024	480785632	914386276	1633145568
PI_v	2592	17568	60480	152928	322560	603072	1034208	1661760	2537568	3719520
PI_e	2754	20052	71150	183072	390618	736364	1270662	2051640	3145202	4625028
Mo_v	1068	8424	29196	74992	158172	297416	509916	821808	1254732	1842664
Mo_e	1242	10216	35898	93160	197530	373224	641658	1037032	1586010	2333416

3.2. Szeged-type entropies of GC strutures

Entropy is an essential concept that quantifies the level of disorder, randomness, or uncertainty within a system. In the field of thermodynamics, it quantifies unusable thermal energy and reflects the system's tendency to become more disordered. In information theory, it measures uncertainty in outcomes, representing information content. In both contexts, entropy describes inherent randomness and the drive towards greater disorder or uncertainty [68]. Shannon's entropy serves as a widely-utilized graph measure that assigns probabilities to components, enabling a more profound comprehension of structural information [69,70]. These entropy-based methods, valued for their capacity to assess system complexity through user-friendly evaluation procedures, hold a prominent role in tackling challenges spanning diverse domains such as computational physics, information theory, thermodynamics, chemistry, statistics, and computer science [71–73].

Table 2
Shannon Szeged-type entropies of P-GC(h).

I_{TI} \ h	1	2	3	4	5	6	7	8	9	10
Sz_v	4.544	5.434	5.988	6.403	6.738	7.020	7.264	7.479	7.672	7.846
Sz_e	4.468	5.364	5.916	6.333	6.670	6.954	7.200	7.418	7.613	7.790
PI_v	4.168	5.109	5.715	6.170	6.536	6.843	7.108	7.341	7.550	7.738
PI_e	4.159	5.095	5.700	6.155	6.522	6.830	7.096	7.330	7.539	7.727
Mo_v	3.442	4.734	5.376	5.862	6.242	6.562	6.835	7.075	7.289	7.482
Mo_e	3.549	4.734	5.369	5.862	6.238	6.561	6.833	7.075	7.287	7.482

Table 3
Modified Shannon Szeged-type entropies of P-GC(h).

I^*_{TI} \ h	1	2	3	4	5	6	7	8	9	10
Sz_v	9.725	12.399	14.356	15.736	16.910	17.846	18.688	19.399	20.062	20.630
Sz_e	9.756	12.590	14.627	16.048	17.254	18.209	19.069	19.792	20.450	21.042
PI_v	7.722	9.676	10.932	11.871	12.625	13.302	13.802	14.280	14.706	15.091
PI_e	7.705	9.701	11.028	11.978	12.763	13.400	13.962	14.443	14.882	15.269
Mo_v	6.716	8.795	10.067	11.035	11.799	12.445	12.995	13.483	13.920	14.306
Mo_e	6.865	8.978	10.266	11.245	12.031	12.666	13.229	13.716	14.145	14.539

Table 4
Normalized Szeged-type indices.

TI \ h	1	2	3	4	5	6	7	8	9	10
Sz_v	20.042	50.288	92.057	145.323	210.063	286.260	373.908	473.000	583.533	705.504
Sz_e	20.347	55.732	105.926	170.870	250.541	344.927	454.022	577.823	716.326	869.532
PI_v	6.928	11.045	14.967	18.815	22.627	26.420	30.199	33.971	37.736	41.497
PI_e	7.141	11.800	16.233	20.586	24.900	29.194	33.474	37.746	42.012	46.273
Mo_v	4.447	7.649	10.399	13.176	15.845	18.554	21.205	23.889	26.535	29.208
Mo_e	4.796	8.423	11.531	14.685	17.707	20.784	23.787	26.836	29.833	32.868

To integrate Shannon's entropy idea and topological indices, we need to identify the structural information function on the elements of $E(\mathrm{GC})$. Such a function can be defined by the structural characteristics of GC by the index function $g : E(\mathrm{GC}) \to \mathbb{R}_+$. Suppose $E(\mathrm{GC}) = \{q_1, q_2, ..., q_n\}$, the Shannon entropy topological index of GC connected to g is given by

$$I_g(\mathrm{GC}) = -\sum_{i=1}^{n} \frac{g(q_i)}{\sum_{j=1}^{n} g(q_j)} \log\left(\frac{g(q_i)}{\sum_{j=1}^{n} g(q_j)}\right) \tag{2}$$

$$= \log\left(\sum_{i=1}^{n} g(q_i)\right) - \frac{1}{\sum_{i=1}^{n} g(q_i)} \log\left(\prod_{i=1}^{n} g(q_i)^{g(q_i)}\right). \tag{3}$$

It is highly uncommon to see that the elements of the set $\{g(q_1), g(q_2), ..., g(q_n)\}$ are distinct, and hence, we rearrange the elements of the set with frequencies as $\{(g_i, r_i) : 1 \le i \le k\}$ where the index value g_i repeated r_i times such that $r_1 + r_2 + ... + r_k = n$. Therefore,

$$I_g(\mathrm{GC}) = \log\left(\sum_{i=1}^{k} r_i g_i\right) - \frac{1}{\sum_{i=1}^{k} r_i g_i} \log\left(\prod_{i=1}^{k} {g_i}^{g_i r_i}\right). \tag{4}$$

In recent studies [74,75], the above defined Shannon entropy topological index was modified by incorporating the scalar multiplication as defined below:

$$I^*_g(\mathrm{GC}) = \log\left(\sum_{i=1}^{k} r_i g_i\right) - \frac{1}{\sum_{i=1}^{k} r_i g_i} \log\left(\prod_{i=1}^{k} r_i {g_i}^{g_i}\right). \tag{5}$$

We now conduct a comparative study between Szeged-type topological indices and Shannon entropy Szeged-type indices as well as with modified entropy indices from Tables 2 and 3. As we see that the numerical values of Szeged-type topological indices are high compared to entropy indices, therefore, we implement data scaling on the Szeged indices to address this disparity based on the number of edges, because these indices were computed with their edge contributions. For this purpose, we calculate the normalized Szeged-type indices for the values in Table 1. This is done by dividing each value by the total number of edges corresponding to its respective dimension, followed by taking the square root. The results are presented in Table 4.

Table 5
Correlation analysis between Shannon entropy and its modified entropy of P-GC(h).

P-GC(h)	Correlation between normalized Szeged index and Shannon entropy	Correlation between normalized Szeged index and modified entropy
$h=1$	0.84250	0.98590
$h=2$	0.85817	0.98390
$h=3$	0.82757	0.98958
$h=4$	0.80695	0.99044
$h=5$	0.78208	0.99077
$h=6$	0.76141	0.99055
$h=7$	0.73948	0.99104
$h=8$	0.71970	0.99114
$h=9$	0.69960	0.99101
$h=10$	0.68084	0.99119

From Table 5, we observe that the correlation values derived using the modified version of Shannon's entropy formula, which incorporates scalar multiplicative indices, demonstrating superior predictive efficacy compared to conventional Shannon's entropy measures. This suggests that integrating modified entropies into the regression model enhances its predictive capability for the normalized Szeged index, consequently leading to an improved accuracy in predicting the physicochemical properties of GC structures.

3.3. Degree topological indices

Degree indices are defined according to the degrees of bond ends. The general formulation of degree topological indices of BT-GC(m,h) is expressed as follows:

$$\chi(\text{BT-GC}) = \sum_{p_1p_2 \in E(\text{BT-GC})} \chi(p_1p_2) \tag{6}$$

where $\chi(p_1p_2) = \chi(p_2p_1)$. The degree topological indices are obtained by taking $\chi(p_1p_2) = \chi(d_{GC}(p_1), d_{GC}(p_2))$ which received a lot of interest [76], including,

- Bi−Zagreb $BM(d_{GC}(p_1), d_{GC}(p_2)) = (d_{GC}(p_1) + d_{GC}(p_2) + d_{GC}(p_1)d_{GC}(p_2))$
- Tri−Zagreb $TM(d_{GC}(p_1), d_{GC}(p_2)) = (d^2_{GC}(p_1) + d^2_{GC}(p_2) + d_{GC}(p_1)d_{GC}(p_2))$
- Geometric−arithmetic $GA(d_{GC}(p_1), d_{GC}(p_2)) = 2\frac{\sqrt{d_{GC}(p_1)d_{GC}(p_1)}}{d_{GC}(p_1) + d_{GC}(p_2)}$
- Geometric−Bi Zagreb $GBM(d_{GC}(p_1), d_{GC}(p_2)) = \frac{\sqrt{d_{GC}(p_1)d_{GC}(p_2)}}{d_{GC}(p_1)+d_{GC}(p_2)+d_{GC}(p_1)d_{GC}(p_2)}$
- Geometric−Tri Zagreb $GTM(d_{GC}(p_1), d_{GC}(p_2)) = \frac{\sqrt{d_{GC}(p_1)d_{GC}(p_2)}}{d^2_{GC}(p_1)+d^2_{GC}(p_2)+d_{GC}(p_1)d_{GC}(p_2)}$
- Bi Zagreb− Geometric $BMG(d_{GC}(p_1), d_{GC}(p_2)) = \frac{d_{GC}(p_1)+d_{GC}(p_2)+d_{GC}(p_1)d_{GC}(p_2)}{\sqrt{d_{GC}(p_1)d_{GC}(p_2)}}$
- Tri Zagreb− Geometric $TMG(d_{GC}(p_1), d_{GC}(p_2)) = \frac{d^2_{GC}(p_1)+d^2_{GC}(p_2)+d_{GC}(p_1)d_{GC}(p_2)}{\sqrt{d_{GC}(p_1)d_{GC}(p_2)}}$
- Harmonic $H(d_{GC}(p_1), d_{GC}(p_2)) = \frac{2}{d_{GC}(p_1) + d_{GC}(p_2)}$
- Sombor $SO(d_{GC}(p_1), d_{GC}(p_2)) = \sqrt{d^2_{GC}(p_1) + d^2_{GC}(p_2)}$
- Atom bond connectivity $ABC(d_{GC}(p_1), d_{GC}(p_2)) = \sqrt{\frac{d_{GC}(p_1) + d_{GC}(p_2) - 2}{d_{GC}(p_1)d_{GC}(p_2)}}$

The topological expressions are derived using the edge partition method applied to the BT-GC(m,h) structure, utilizing the degrees of the endpoints of the edges. The partition of the bond set of BT-GC(m,h) is shown in Table 6. In our topological expressions, we employ three classes based on the degrees of their endpoints, namely $(1,3),(2,3)$ and $(3,3)$, with respective cardinalities of $4h+4m+4$, $24hm - 12h^2 + 20h - 4m - 4$ and $12hm - 6h^2 + 12h$.

Theorem 3. *The degree topological indices of* BT-GC(m,h) *are given by*

1. $BM(\text{BT-GC}(m,h)) = 444hm - 222h^2 + 428h - 16m - 16$,

2. $TM(\text{BT-GC}(m,h)) = 780hm - 390h^2 + 756h - 24m - 24$,
3. $GA(\text{BT-GC}(m,h)) = \frac{2}{5}(24\sqrt{6}hm + 30hm - 12\sqrt{6}h^2 - 15h^2 + 20\sqrt{6}h + 5\sqrt{3}h + 30h - 4\sqrt{6}m + 5\sqrt{3}m - 4\sqrt{6} + 5\sqrt{3})$,
4. $GBM(\text{BT-GC}(m,h)) = \frac{2}{385}(420\sqrt{6}hm + 462hm - 210\sqrt{6}h^2 - 231h^2 + 110\sqrt{3}h + 350\sqrt{6}h + 462h + 110\sqrt{3}m - 70\sqrt{6}m + 110\sqrt{3} - 70\sqrt{6})$,
5. $GTM(\text{BT-GC}(m,h)) = \frac{2}{741}(468\sqrt{6}hm + 494hm - 234\sqrt{6}h^2 - 247h^2 + 114\sqrt{3}h + 390\sqrt{6}h + 494h + 114\sqrt{3}m - 78\sqrt{6}m + 114\sqrt{3} - 78\sqrt{6})$,
6. $BMG(\text{BT-GC}(m,h)) = \frac{2}{3}(66\sqrt{6}hm + 90hm - 33\sqrt{6}h^2 - 45h^2 + 55\sqrt{6}h + 14\sqrt{3}h + 90h - 11\sqrt{6}m + 14\sqrt{3}m - 11\sqrt{6} + 14\sqrt{3})$,
7. $TMG(\text{BT-GC}(m,h)) = \frac{2}{3}(114\sqrt{6}hm + 162hm - 57\sqrt{6}h^2 - 81h^2 + 95\sqrt{6}h + 26\sqrt{3}h + 162h - 19\sqrt{6}m + 26\sqrt{3}m - 19\sqrt{6} + 26\sqrt{3})$,
8. $H(\text{BT-GC}(m,h)) = \frac{2}{5}(34hm - 17h^2 + 35h + m + 1)$,
9. $SO(\text{BT-GC}(m,h)) = 2(18\sqrt{2}hm + 12\sqrt{13}hm - 9\sqrt{2}h^2 - 6\sqrt{13}h^2 + 18\sqrt{2}h + 2\sqrt{10}h + 10\sqrt{13}h + 2\sqrt{10}m - 2\sqrt{13}m + 2\sqrt{10} - 2\sqrt{13})$,
10. $ABC(\text{BT-GC}(m,h)) = \frac{2}{3}(18\sqrt{2}hm + 12hm - 9\sqrt{2}h^2 - 6h^2 + 2\sqrt{6}h + 15\sqrt{2}h + 12h + 2\sqrt{6}m - 3\sqrt{2}m + 2\sqrt{6} - 3\sqrt{2})$.

Table 6
Degree bond partition of BT-GC(m,h).

Bond-type X−Y	$d_{GC}(X)$-$d_{GC}(Y)$	Number of occurrences in BT-GC(m,h)
O−H N−H	1 − 3 1 − 3	$2h + 2m + 2$
O−H N−H	2 − 3 2 − 3	$12hm - 6h^2 + 10h - 2m - 2$
O−C N−C	3 − 3 3 − 3	$6hm - 3h^2 + 6h$

Table 7
Degree based entropies of P-GC(h).

I^*_{TI} \ h	1	2	3	4	5	6	7	8	9	10
BM	6.282	7.382	8.048	8.535	8.923	9.245	9.521	9.764	9.979	10.174
TM	6.831	7.943	8.611	9.100	9.488	9.810	10.087	10.329	10.544	10.739
GA	3.788	4.861	5.525	6.012	6.380	6.723	7.000	7.241	7.457	7.651
GBM	1.844	3.125	3.872	4.402	4.814	5.152	5.440	5.689	5.910	6.109
GTM	0.739	2.293	3.144	3.726	4.169	4.526	4.827	5.086	5.314	5.518
BMG	5.389	6.448	7.101	7.582	7.966	8.286	8.561	8.801	9.016	9.209
TMG	5.947	7.013	7.667	8.148	8.531	8.851	9.125	9.366	9.580	9.773
H	2.727	3.853	4.540	5.039	5.433	5.759	6.038	6.282	6.499	6.694
SO	5.188	6.246	6.899	7.381	7.765	8.085	8.360	8.601	8.816	9.009
ABC	3.455	4.523	5.185	5.672	6.058	6.380	6.656	6.898	7.113	7.307

We now derive the entropy measures associated with those degree based topological indices of GC structure. The numerical values are given in Table 7, and corresponding 3-D bar plots generated with the MATLAB interface are shown in Fig. 6.

3.4. Existence of isentropic GC structures

In the context of graph theory and molecular chemistry, isentropic structures represent arrangements within molecular systems or data sets that exhibit a constant level of entropy or information content. They have significance in both thermodynamics and information theory and can be valuable for understanding the behavior of complex systems in various scientific and engineering disciplines.

In the computation of degree indices, we encountered that multiple structures exhibited the same number of GC units, vertices, edges, and edge partitions indicating identical degree topological properties, yet different distance properties. We found several isentropic structures and described as pair in the following general form: (BT-GC$(5m-4,m)$, BT-GC$(3m-2,3m-2)$), $m \geq 2$. Table 8 provides numerical bond partition values for some isentropic structures, and Fig. 7(a-b) exhibits one such isentropic structures.

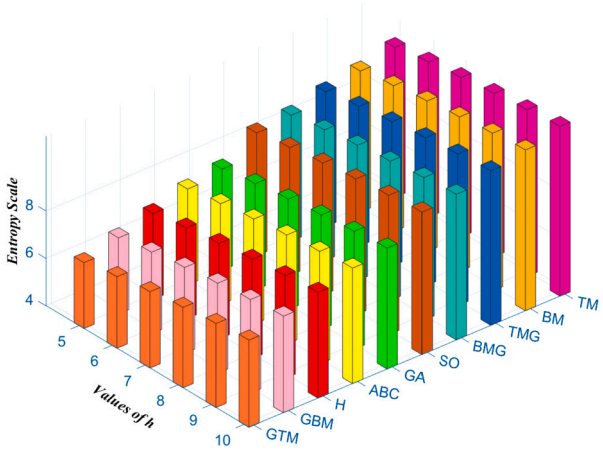

Fig. 6. Degree-entropies of P-GC(h).

Table 8
Numerical bond partition values of isentropic structures of BT-GC(m, h).

Bond-type X–Y	$d_{GC}(X)$-$d_{GC}(Y)$	Isentropic Structures								
		(6,2)	(4,4)	(11,3)	(7,7)	(16,4)	(10,10)	(21,5)	(13,13)	(26,6)	(16,16)
O–H N–H	1 – 3 1 – 3	18		30		42		54		66	
O–H N–H	2 – 3 2 – 3	126		348		678		1116		1662	
O–C N–C	3 – 3 3 – 3	72		189		360		585		864	

4. Proton, ^{13}C, ^{14}N, ^{17}O NMR combinatorial spectroscopic patterns for four different supramolecular assemblies of guanidinium and hydrogen carbonate rosettes

As networks comprised of guanidinium and hydrogen carbonate rosettes, contain different nuclei such as protons, carbons, nitrogens, and oxygens, once can harness different NMR spectroscopies to contrast closely related networks. As shown in the previous section, these networks not only exhibit isentropic structures but also isomeric structures. Due to the considerable complexity of these supramolecular assemblies, there is a clear and compelling need to develop graph-theoretical and combinatorial methods for the enumeration and construction of different NMR spectral patterns such as proton NMR, ^{13}C NMR, ^{14}N NMR and ^{17}O NMR. Through the use of such powerful techniques, the isomers and isentropic structures can be experimentally contrasted using a variety of NMR techniques. Hence, we describe the salient points pertinent to these graph theoretical and combinatorial methods for NMR.

The distance degree sequence vector (DDSV) for a vertex [77] in the supramolecular hydrogen-bonded network of guanidinium and hydrogen carbonate rosettes is defined as $(d_{i0}, d_{i1}, d_{i2}, \ldots, d_{ij}, \ldots)$ where a vertex v_i in GC, d_{ij} is the number of vertices at distance j from v_i. The sequence terminates for a vertex v of the graph at $ecc(v)$, where $ecc(v)$ is the eccentricity of the vertex v. We note that in the usual graph theoretical methods, hydrogens are omitted, but because the supramolecular assemblies of guanidinium and hydrogen carbonate rosettes are formed with hydrogen bonds, in the ensuing graph theoretical and combinatorial methods, the hydrogens are explicitly included in graphs. In this method, we use TopoChemie 2020 software [78] to compute the number of vertices at a given distance from the vertex v_i, by making use of the distance matrices generated by the codes. Hence, a vector sequence is generated for each vertex, including the hydrogens. Such a sequence is of variable length, as the eccentricities of various vertices in the supramolecular assembly are never the same for all vertices. Then the code analyzes the vector sequence thus generated and assigns it to each vertex, and if two vertices carry the same DDSV label, then they are assigned to the same equivalence class. Consequently, the DDSV technique facilitates partitioning to first order the various nuclei of guanidinium and hydrogen carbonate rosettes into equivalence classes of nuclei. We note that the DDSV-partitions are not isomorphic to the automorphic partitions. However for guanidinium and hydrogen carbonate rosettes, they provide a starting point to refine the partition classes further. As heteroatoms are not contrasted with carbons and because hydrogens are also included as vertices in the graph, the DDSV technique at best yields a starting point for the generation of equivalence classes through further symmetry-based combinatorial refinement. Consequently, we have invoked further symmetry-based combinatorial techniques that are adequately described elsewhere [79–81] to generate the various nuclear partitions and thus the NMR spectral patterns of these networks. It is noted that there are large numbers of nuclei for the supramolecular assemblies considered here, and because each nucleus gives rise to a vector of variable DDSV length, the process of generating the nuclear partitions becomes cumbersome, and requires machine-algorithms which were implemented.

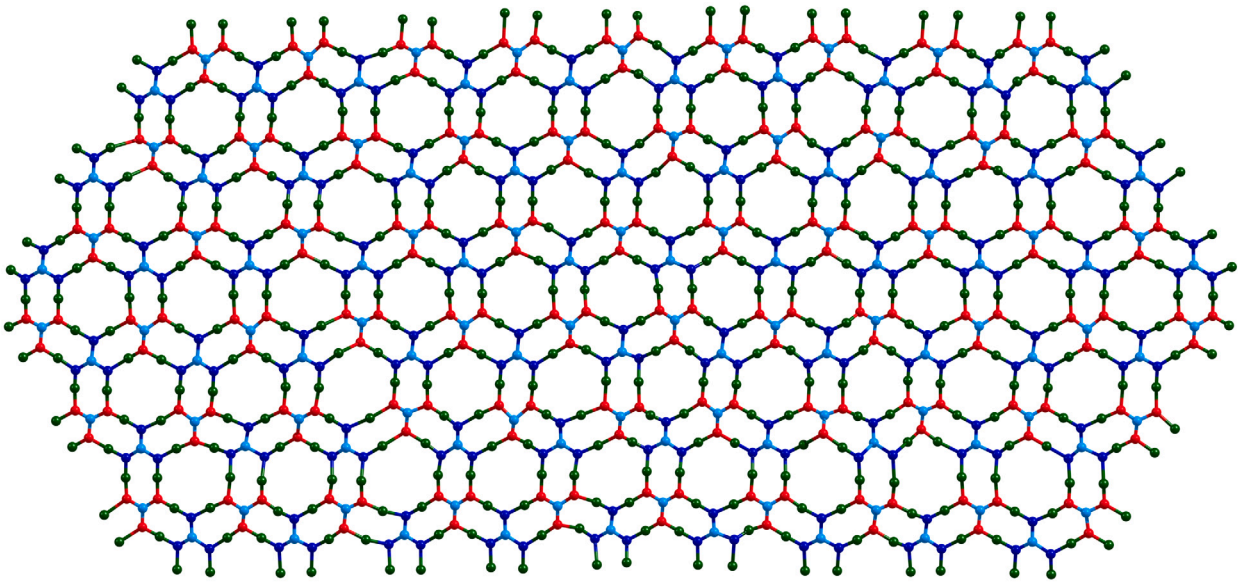

(a)

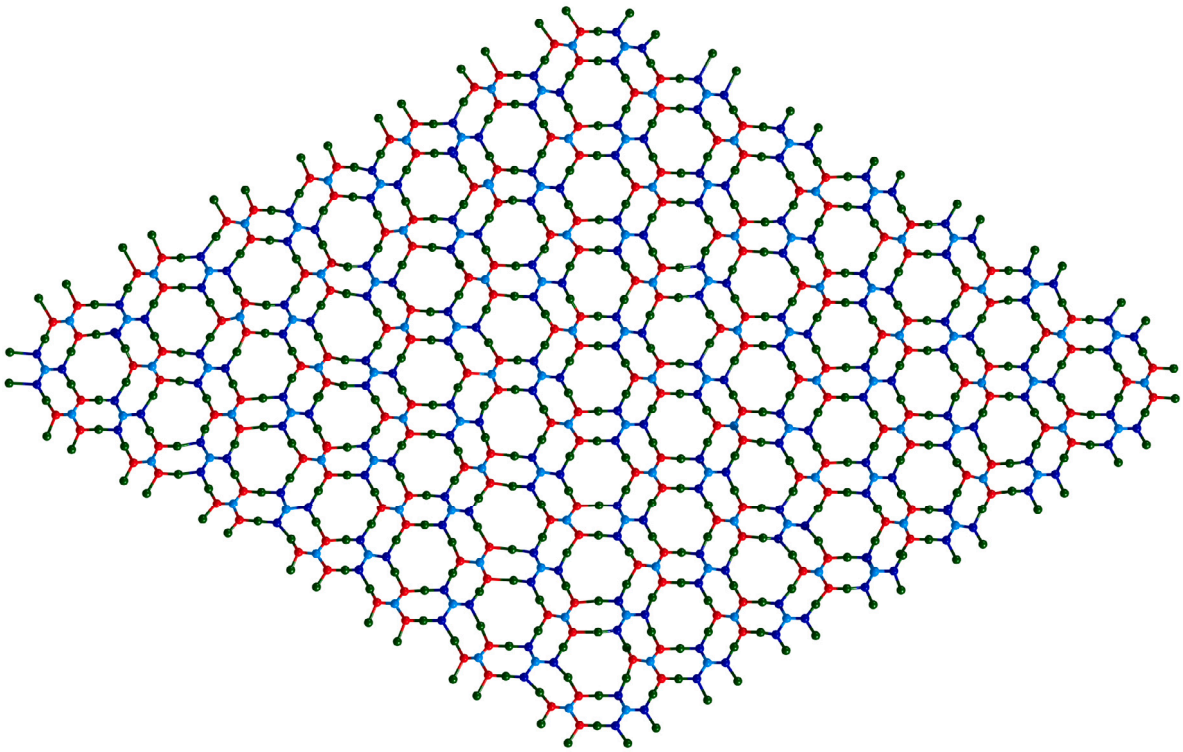

(b)

Fig. 7. Isentropic structures (a) BT-GC(11, 3) (b) BT-GC(7, 7).

Such algorithms are part of the TopoChemie-2020 package [78] which was also employed to validate the expressions obtained for all topological indices and entropies considered in this study. We have computed the machine-generated nuclear equivalence classes and the NMR intensity and signal patterns for the proton, ^{13}C, ^{14}N, and ^{17}O of four structures supramolecular assemblies of guanidinium and hydrogen carbonate rosettes, which are shown in Fig. 8(a-d).

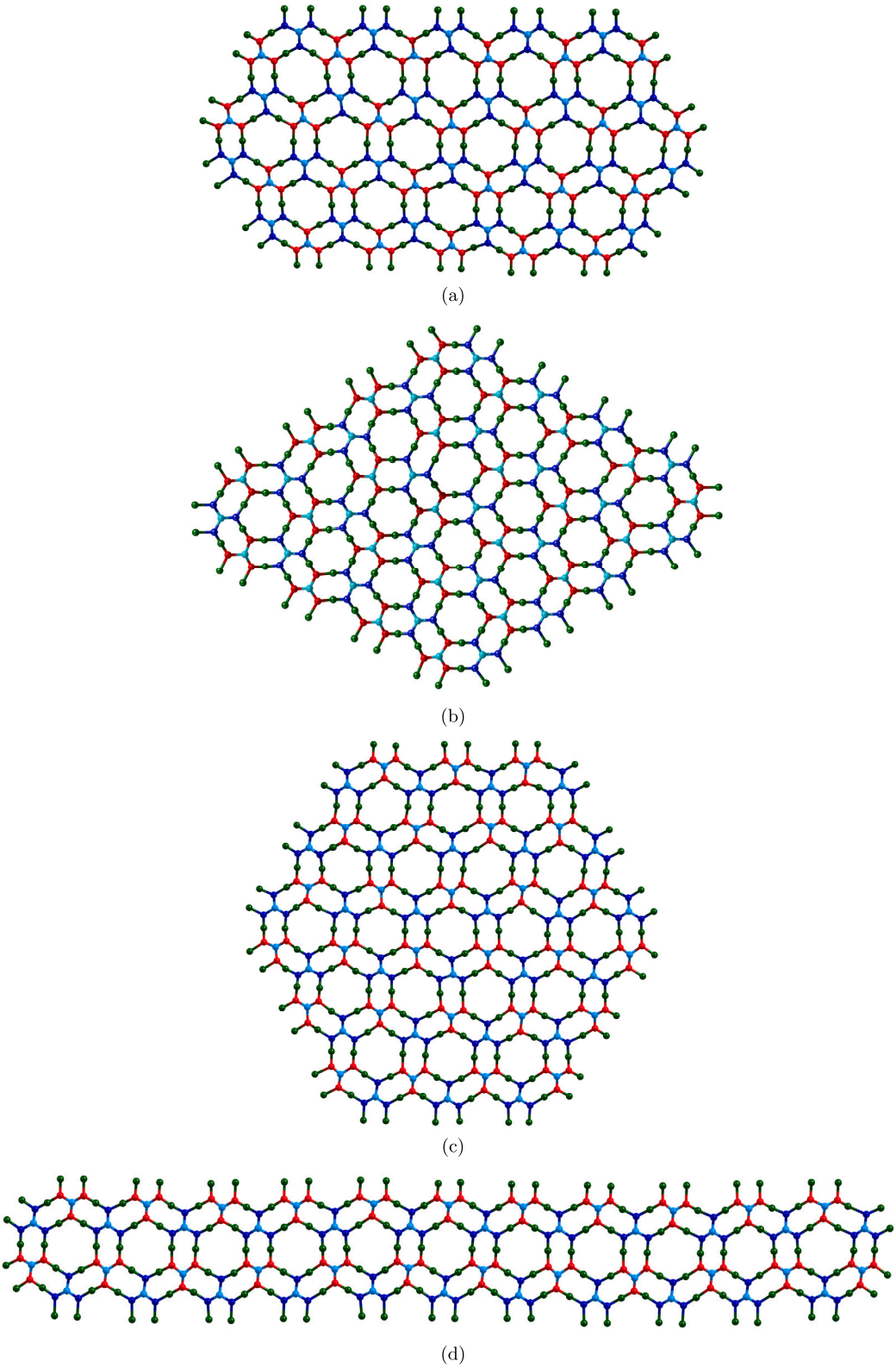

Fig. 8. Four GC structures (a) BT-GC(6, 2) (b) BT-GC(4, 4) (c) BT-GC(5, 3) (d) BT-GC(11, 1). The first two structures are isomers. Their machine-generated NMR patterns are displayed in Table 9.

Table 9
Machine-generated proton, ^{13}C, ^{14}N, and ^{17}O NMR spectral patterns of four different supramolecular assemblies of guanidinium and hydrogen carbonate rosettes.

BT-GC(m,h)	Molecular Formulas	Proton Classes and NMR	^{13}C Classes and ^{13}C NMR	^{14}N Classes and ^{14}N NMR	^{17}O Classes and ^{17}O NMR
BT-GC(6, 2) Fig. 8a	$C_{48}H_{162}N_{72}O_{72}$	2^{81} 1 : 1 : ⋯ : 1 : 1(81)	$1^4 2^{22}$ 1 : 1 : 1 : 1 2 : 2 : ⋯ : 2(22)	$1^2 2^{35}$ 1 : 1 2 : 2 : ⋯ : 2(35)	$1^2 2^{35}$ 1 : 1 2 : 2 : ⋯ : 2(35)
BT-GC(4, 4) Fig. 8b	$C_{48}H_{162}N_{72}O_{72}$	2^{81} 1 : 1 : ⋯ : 1 : 1(81)	$1^8 2^{20}$ 1 : 1 : ⋯ : 1 : 1(8) 2 : 2 : ⋯ : 2 : 2(20)	$1^4 2^{34}$ 1 : 1 : 1 : 1 2 : 2 : ⋯ : 2(34)	$1^4 2^{34}$ 1 : 1 : 1 : 1 2 : 2 : ⋯ : 2(34)
BT-GC(5, 3) Fig. 8c	$C_{54}H_{180}N_{81}O_{81}$	6^{30} 1 : 1 : ⋯ : 1(30)	$3^6 6^6$ 1 : 1 : 1 : 1 : 1 : 1 2 : 2 : 2 : 2 : 2 : 2	$3^3 6^{12}$ 1 : 1 : 1 : 2 : 2 : … 2(12)	$3^3 6^{12}$ 1 : 1 : 1 : 2 : 2 : ⋯ : 2(12)
BT-GC(11, 1) Fig. 8d	$C_{46}H_{164}N_{69}O_{69}$	2^{82} 1 : 1 : ⋯ : 1(82)	$1^2 2^{22}$ 1 : 1 : 2 : 2 : ⋯ : 2(22)	$1\,2^{34}$ 1 : 2 : 2 : ⋯ : 2(34)	$1\,2^{34}$ 1 : 2 : 2 : ⋯ : 2(34)

As one can see from Table 9, different NMR spectroscopies offer powerful tools to characterize the various supramolecular assemblies of guanidinium and hydrogen carbonate rosettes including isomers. For example, the BT-GC(6, 2) and BT-GC(4, 4) structures shown in Fig. 8a and Fig. 8b, respectively are isomers. Their proton NMR spectral patterns, as inferred from the machine-computed NMR spectra, are identical for the two isomers yielding 81 proton NMR signals of equal intensity for both isomers. Consequently, the proton NMR spectroscopy fails to offer any discrimination between the two isomers.

On the other hand, the ^{13}C NMR spectroscopy offers a powerful tool to contrast these two isomers although the ^{14}N and ^{17}O NMR are predicted to be identical for each of the two isomers, they do offer contrast between the isomers (see Table 9). That is for the isomer in Fig. 8a, the ^{13}C NMR four signals of equal unit intensity while there are 22 signals with double the intensity. On the other hand, the ^{13}C NMR for Fig. 8b is predicted to yield 8 signals of equal unit intensities and 20 signals of double intensity, thereby offering a contrast between the isomers in Fig. 8a and Fig. 8b. For the last two structures in Table 9, likewise proton and ^{13}C NMR offer powerful tools to elucidate these structures while ^{14}N and ^{17}O NMR for each structure exhibit the same pattern. This is evidently a consequence of how the different atoms are networked in the structures resulting in their overall weighted-graph symmetries and automorphic partitions. Therefore it is concluded that either ^{14}N or ^{17}O NMR may be employed to study the various assemblies of these structures but not both as the two NMR spectroscopies yield the same information. On the other hand, ^{13}C NMR spectroscopy offers a powerful tool for the elucidation of various assemblies of these structures.

5. Conclusion

In this study, we explored guanidinium and hydrogen carbonate rosette layers, revealing their unique structural properties through topological indices. We employed the cut method technique to dissect their complex structures and used distance and degree based topological indices and Szeged-type and degree entropies for analysis. In the correlation analysis, we found that the modified Shannon entropy exhibits a stronger correlation compared to traditional Shannon entropy. Moreover our studies have revealed the existence of isentropic assemblies and isomeric assemblies in GC structures. Furthermore, we have developed methods that utilize distance degree vector sequences in combination with symmetry-based combinatorial techniques to produce a diverse range of NMR spectral patterns for these networks, including proton, ^{13}C, ^{14}N, and ^{17}O NMR spectra. It is shown that the ^{13}C NMR is powerful methods that facilitates delineation of closely related isomers of assemblies of these structures. Moreover, ^{17}O and ^{14}N NMR spectra for each of the these assemblies produce identical signal and intensity patterns. This research not only enhances our comprehension of these intriguing systems but also underscores the pivotal role of supramolecular chemistry in designing functional materials and advancing molecular self-assembly processes. As we continue to explore the potential of non-covalent interactions, these findings hold promise for innovative applications across diverse scientific domains.

CRediT authorship contribution statement

Micheal Arockiaraj: Writing – review & editing, Supervision, Methodology, Conceptualization. **J. Celin Fiona:** Writing – original draft, Visualization, Investigation, Formal analysis. **Jessie Abraham:** Writing – original draft, Methodology, Investigation, Formal analysis. **Sandi Klavžar:** Writing – original draft, Methodology, Formal analysis, Conceptualization. **Krishnan Balasubramanian:** Writing – review & editing, Validation, Methodology, Formal analysis.

Declaration of competing interest

The authors declare that they have no known competing financial interests or personal relationships that could have appeared to influence the work reported in this paper.

Data availability

All data used for the research are contained in the article.

References

[1] M. Lin, Y. Dai, F. Xia, X. Zhang, Advances in non-covalent crosslinked polymer micelles for biomedical applications, Mater. Sci. Eng. C, Mater. Biol. Appl. 119 (2021) 111626.
[2] I. Alkorta, J. Elguero, A. Frontera, Not only hydrogen bonds: other noncovalent interactions, Crystals 10 (2020) 180.
[3] S. Jena, J. Dutta, K.D. Tulsiyan, A.K. Sahu, S.S. Choudhury, H.S. Biswal, Noncovalent interactions in proteins and nucleic acids: beyond hydrogen bonding and π-stacking, Chem. Soc. Rev. 51 (2022) 4261–4286.
[4] V.R. Mundlapati, D.K. Sahoo, S. Bhaumik, S. Jena, A. Chandrakar, H.S. Biswal, Noncovalent carbon-bonding interactions in proteins, Angew. Chem., Int. Ed. Engl. 57 (2018) 16496–16500.
[5] M.C. Jarvis, Hydrogen bonding and other non-covalent interactions at the surfaces of cellulose microfibrils, Cellulose 30 (2023) 667–687.
[6] I. Alkorta, I. Rozas, J. Elguero, Non-conventional hydrogen bonds, Chem. Soc. Rev. 27 (1998) 163–170.
[7] M. Juanes, R.T. Saragi, W. Caminati, A. Lesarri, The hydrogen bond and beyond: perspectives for rotational investigations of non-covalent interactions, Chem. Eur. J. 25 (2019) 11402–11411.
[8] P.R. Varadwaj, A. Varadwaj, H.M. Marques, K. Yamashita, Significance of hydrogen bonding and other noncovalent interactions in determining octahedral tilting in the $CH_3NH_3PbI_3$ hybrid organic-inorganic halide perovskite solar cell semiconductor, Sci. Rep. 9 (2019) 50.
[9] F. Huang, E.V. Anslyn, Introduction: supramolecular chemistry, Chem. Rev. 115 (2015) 6999–7000.
[10] J.W. Steed, J.L. Atwood, Supramolecular Chemistry, Wiley, 2009.
[11] J.-H. Deng, J. Luo, Y.-L. Mao, S. Lai, Y.-N. Gong, D.-C. Zhong, T.-B. Lu, π-π stacking interactions: non-negligible forces for stabilizing porous supramolecular frameworks, Sci. Adv. 6 (2020) eaax9976.
[12] M. Gobbi, S. Bonacchi, J.X. Lian, Y. Liu, X.-Y. Wang, M.-A. Stoeckel, M.A. Squillaci, G. D'Avino, A. Narita, K. Müllen, X. Feng, Y. Olivier, D. Beljonne, P. Samorì, E. Orgiu, Periodic potentials in hybrid van der Waals heterostructures formed by supramolecular lattices on graphene, Nat. Commun. 8 (2017) 14767.
[13] N.H. Evans, P.D. Beer, Advances in anion supramolecular chemistry: from recognition to chemical applications, Angew. Chem., Int. Ed. Engl. 53 (2014) 11716–11754.
[14] I.V. Kolesnichenko, E.V. Anslyn, Practical applications of supramolecular chemistry, Chem. Soc. Rev. 46 (2017) 2385–2390.
[15] D.-X. Wang, M.-X. Wang, Exploring anion-π interactions and their applications in supramolecular chemistry, Acc. Chem. Res. 53 (2020) 1364–1380.
[16] V. Bhalla, Supramolecular chemistry: from molecule to molecular machines, Resonance 23 (2018) 277–290.
[17] T. Higashi, D. Iohara, K. Motoyama, H. Arima, Supramolecular pharmaceutical sciences: a novel concept combining pharmaceutical sciences and supramolecular chemistry with a focus on cyclodextrin-based supermolecules, Chem. Pharm. Bull. 66 (2018) 207–216.
[18] K. Ariga, T. Kunitake, Supramolecular Chemistry-Fundamentals and Applications: Advanced Textbook, Springer, Heidelberg, 2006.
[19] S. van Dun, C. Ottmann, L.-G. Milroy, L. Brunsveld, Supramolecular chemistry targeting proteins, J. Am. Chem. Soc. 139 (2017) 13960–13968.
[20] A. Barba-Bon, M. Nilam, A. Hennig, Supramolecular chemistry in the biomembrane, ChemBioChem 21 (2019) 886–910.
[21] D.-S. Guo, Y. Liu, Supramolecular chemistry of p-sulfonatocalix[n]arenes and its biological applications, Acc. Chem. Res. 47 (2014) 1925–1934.
[22] X. Ma, Y. Zhao, Biomedical applications of supramolecular systems based on host–guest interactions, Chem. Rev. 115 (2015) 7794–7839.
[23] D.A. Cullen, M.G. Gardiner, N.G. White, A three dimensional hydrogen bonded organic framework assembled through antielectrostatic hydrogen bonds, Chem. Commun. 55 (2019) 12020–12023.
[24] G.-G. Luo, D.-L. Wu, L. Liu, J.-X. Xia, D.-X. Li, C. Peng, Z.-J. Xiao, J.-C. Dai, The first supramolecular water–borate–carbonate anionic rosette ribbon sandwiched by a Ag(I) cationic sinusoidal layer, Inorg. Chem. Commun. 15 (2012) 272–276.
[25] J. Han, C.-W. Yau, C.-K. Lam, T.C.W. Mak, Designed supramolecular assembly of hydrogen-bonded anionic rosette layers, J. Am. Chem. Soc. 130 (2008) 10315–10326.
[26] I. Insua, J. Montenegro, Synthetic supramolecular systems in life-like materials and protocell models, Chem. 6 (2020) 1652–1682.
[27] Y. Lin, C. Mao, Bio-inspired supramolecular self-assembly towards soft nanomaterials, Front. Mater. Sci. 5 (2011) 247–265.
[28] J.M. Withers, G. Padroni, S.M. Pauff, A.W. Clark, S.P. Mackay, G.A. Burley, DNA minor groove binders as therapeutic agents, in: Comprehensive Supramolecular Chem. II, vol. 5, 2017, pp. 149–178.
[29] S.I. Stupp, L.C. Palmer, Supramolecular chemistry and self-assembly in organic materials design, Chem. Mater. 26 (2014) 507–518.
[30] Q. Song, Z. Cheng, M. Kariuki, S.C.L. Hall, S.K. Hill, J.Y. Rho, S. Perrier, Molecular self-assembly and supramolecular chemistry of cyclic peptides, Chem. Rev. 121 (2021) 13936–13995.
[31] K. Balasubramanian, Computational and artificial intelligence techniques for drug discovery and administration, Compr. Adv. Pharmacol. 2 (2022) 553–616.
[32] K. Balasubramanian, Mathematical and computational techniques for drug discovery: promises and developments, Curr. Top. Med. Chem. 18 (2019) 2774–2799.
[33] K. Balasubramanian, Combinatorics, big data, neural network & AI for medicinal chemistry & drug administration, Lett. Drug. Des. Discov. 18 (2021) 943–948.
[34] K. Balasubramanian, Enumeration of internal-rotation reactions and their reaction graphs, Theor. Chim. Acta 53 (1979) 129–146.
[35] N.G. White, Recent advances in self-assembled amidinium and guanidinium frameworks, Dalton Trans. 48 (2019) 7062–7068.
[36] R.G. Wüstenberg, J.-M. Neudörfl, H.-G. Schmalz, Supramolecular behaviour of N,N'-bridged guanidinium nitrates in the crystalline state: identification of privileged hydrogen bond networks, Isr. J. Chem. 63 (2023) e202300018.
[37] S.V. Jeyaraj, R. Santiago, A study on efficient technique for generating vertex-based topological characterization of boric acid 2D structure, ACS Omega 8 (2023) 23089–23097.
[38] T.C.W. Mak, F. Xue, Supramolecular rosette ribbon constructed from guanidinium and hydrogen carbonate ions in the crystal engineering of hydrogen-bonded networks, J. Am. Chem. Soc. 122 (2000) 9860–9861.
[39] J. Han, C.-W. Yau, C.W. Chan, T.C.W. Mak, Anionic host layers constructed with guanidinium–hydrogen carbonate dimer 2:1 rosette-ribbons and bridging carboxylate connectors, Cryst. Growth Des. 12 (2012) 4457–4465.
[40] C.-K. Lam, F. Xue, J.-P. Zhang, X.-M. Chen, T.C.W. Mak, Hydrogen-bonded anionic rosette networks assembled with guanidinium and C_3-symmetric oxoanion building blocks, J. Am. Chem. Soc. 127 (2005) 11536–11537.
[41] C.-K. Lam, S.C.-K. Hau, C.-W. Yau, T.C.W. Mak, Hydrogen-bonded anionic host lattices constructed with isocyanurate and thiourea/urea, Cryst. Growth Des. 16 (2016) 759–773.
[42] S. Shirakol, M. Kalyanshetti, S.M. Hosamani, QSPR analysis of certain distance based topological indices, Appl. Math. Nonlinear Sci. 4 (2019) 371–386.
[43] S. Nagarajan, G. Priyadharsini, K. Pattabiraman, QSPR modeling of status-based topological indices with COVID-19 drugs, Polycycl. Aromat. Compd. 43 (2023) 6868–6887.
[44] S. Mondal, N. De, A. Pal, Topological indices of some chemical structures applied for the treatment of COVID-19 patients, Polycycl. Aromat. Compd. 42 (2022) 1220–1234.
[45] M. Cancan, S. Ediz, S. Fareed, M.R. Farahani, More topological indices of generalized prism network, J. Inf. Optim. Sci. 41 (2020) 925–932.

[46] M.C. Shanmukha, N.S. Basavarajappa, K.C. Shilpa, A. Usha, Degree-based topological indices on anticancer drugs with QSPR analysis, Heliyon 6 (2020) e04235.
[47] S. Zaman, H.S.A. Yaqoob, A. Ullah, M. Sheikh, QSPR analysis of some novel drugs used in blood cancer treatment via degree based topological indices and regression models, Polycycl. Aromat. Compd. (2023), https://doi.org/10.1080/10406638.2023.2217990.
[48] H. Iqbal, M.H. Aftab, A. Akgul, Z.S. Mufti, I. Yaqoob, M. Bayram, M.B. Riaz, Further study of eccentricity based indices for benzenoid hourglass network, Heliyon 9 (2023) e16956.
[49] S. Hayat, S. Khan, M. Imran, J.B. Liu, Quality testing of distance-based molecular descriptors for benzenoid hydrocarbons, J. Mol. Struct. 1222 (2020) 128927.
[50] S. Prabhu, G. Murugan, M. Arockiaraj, M. Arulperumjothi, V. Manimozhi, Molecular topological characterization of three classes of polycyclic aromatic hydrocarbons, J. Mol. Struct. 1229 (2021) 129501.
[51] Z.-H. Ni, F.-S. Li, H. Wang, H. Xiao, Prediction of physical parameters of Jatropha biodiesel-ethanol dual fuel based on topological indices, Appl. Energy 328 (2022) 120202.
[52] S. Sorgun, H. Küçük, K. Birgin, Some distance-based topological indices of certain polysaccharides, J. Mol. Struct. 1250 (2022) 131716.
[53] M. Arockiaraj, J. Jency, J. Abraham, S. Ruth Julie Kavitha, K. Balasubramanian, Two-dimensional coronene fractal structures: topological entropy measures, energetics, NMR and ESR spectroscopic patterns and existence of isentropic structures, Mol. Phys. 120 (2022) e2079568.
[54] M. Adnan, S.A.U.H. Bokhary, G. Abbas, T. Iqbal, Degree-based topological indices and QSPR analysis of antituberculosis drugs, J. Chem. 2022 (2022) 5748626.
[55] I. Gutman, J. Monsalve, J. Rada, A relation between a vertex-degree-based topological index and its energy, Linear Algebra Appl. 636 (2022) 134–142.
[56] A. Ullah, S. Zaman, A. Hamraz, M. Muzammal, On the construction of some bioconjugate networks and their structural modeling via irregularity topological indices, Eur. Phys. J. E 46 (2023) 72.
[57] T. Yan, Z. Kosar, A. Aslam, S. Zaman, A. Ullah, Spectral techniques and mathematical aspects of K4 chain graph, Phys. Scr. 98 (2023) 045222.
[58] M. Arockiaraj, J. Jency, A. Maaran, J. Abraham, K. Balasubramanian, Refined degree bond partitions, topological indices, graph entropies and machine-generated boron NMR spectral patterns of borophene nanoribbons, J. Mol. Struct. 1295 (2024) 136524.
[59] M. Arockiaraj, S. Klavžar, S. Mushtaq, K. Balasubramanian, Distance-based topological indices of nanosheets, nanotubes and nanotori of SiO_2, J. Math. Chem. 57 (2019) 343–369.
[60] M. Arockiaraj, J. Clement, K. Balasubramanian, Topological indices and their applications to circumcised donut benzenoid systems, kekulenes and drugs, Polycycl. Aromat. Compd. 40 (2018) 280–303.
[61] M. Arockiaraj, J. Clement, N. Tratnik, Mostar indices of carbon nanostructures and circumscribed donut benzenoid systems, Int. J. Quant. Chem. 119 (2019) e26043.
[62] S. Klavžar, M. Nadjafi-Arani, Cut method: update on recent developments and equivalence of independent approaches, Curr. Org. Chem. 19 (2015) 348–358.
[63] S. Klavžar, On the canonical metric representation, average distance, and partial Hamming graphs, Eur. J. Comb. 27 (2006) 68–73.
[64] M. Dehmer, F. Emmert-Streib, N. Tratnik, P. Žigert Pleteršek, Szeged-like entropies of graphs, Appl. Math. Comput. 431 (2022) 127325.
[65] N. Tratnik, Computing weighted Szeged and PI indices from quotient graphs, Int. J. Quant. Chem. 119 (2019) e26006.
[66] S. Klavžar, I. Gutman, B. Mohar, Labeling of benzenoid systems which reflects the vertex-distance relations, J. Chem. Inf. Comput. Sci. 35 (1995) 590–593.
[67] S. Klavžar, M.J. Nadjafi-Arani, Wiener index in weighted graphs via unification of Θ^*-classes, Eur. J. Comb. 36 (2014) 71–76.
[68] A. Sciacovelli, V. Verda, E. Sciubba, Entropy generation analysis as a design tool-a review, Renew. Sustain. Energy Rev. 43 (2015) 1167–1181.
[69] M. Dehmer, A. Mowshowitz, Generalized graph entropies, Complexity 17 (2011) 45–50.
[70] A. Mowshowitz, M. Dehmer, Entropy and the complexity of graphs revisited, Entropy 14 (2012) 559–570.
[71] M. Dehmer, A. Mowshowitz, A history of graph entropy measures, Inf. Sci. 181 (2011) 57–78.
[72] M. Ribeiro, T. Henriques, L. Castro, A. Souto, L. Antunes, C. Costa-Santos, A. Teixeira, The entropy universe, Entropy 23 (2021) 222.
[73] C. Feng, M.H. Muhamad, M.K. Siddiqui, S.A.K. Kirmani, S. Manzoor, M.F. Hanif, On entropy measures for molecular structures of remdesivir system and their applications, Int. J. Quant. Chem. 122 (2022) e26957.
[74] S.R.J. Kavitha, J. Abraham, M. Arockiaraj, J. Jency, K. Balasubramanian, Topological characterization and graph entropies of tessellations of kekulene structures: existence of isentropic structures and applications to thermochemistry, NMR and ESR, J. Phys. Chem. A 125 (2021) 8140–8158.
[75] J. Abraham, M. Arockiaraj, J. Jency, S.R.J. Kavitha, K. Balasubramanian, Graph entropies, enumeration of circuits, walks and topological properties of three classes of isoreticular metal organic frameworks, J. Math. Chem. 60 (2022) 695–732.
[76] M. Arockiaraj, D. Paul, J. Clement, S. Tigga, K. Jacob, K. Balasubramanian, Novel molecular hybrid geometric-harmonic-Zagreb degree based descriptors and their efficacy in QSPR studies of polycyclic aromatic hydrocarbons, SAR QSAR Environ. Res. 34 (2023) 569–589.
[77] G.S. Bloom, J.W. Kennedy, L.V. Quintas, Some problems concerning distance and path degree sequences, in: M. Borowiecki, J.W. Kennedy, M.M. Syslo (Eds.), Graph Theory, in: Lecture Notes in Mathematics, vol. 1018, 1983, pp. 179–190.
[78] K. Balasubramanian, Topochemie-2020-A Fortan 95 Package (Software). A computational package for computing topological indices, spectral polynomials, walks and distance degree sequences and combinatorial generators, 2020.
[79] K. Balasubramanian, Combinatorial enumeration of stereo, chiral and position isomers of polysubstituted halocarbons: applications to machine learning of proton and ^{35}Cl NMR spectroscopy of halocarbons, Theor. Chem. Acc. 140 (2021) 58.
[80] K. Balasubramanian, Computer perception of NMR symmetry, J. Magn. Reson., Ser. A 112 (1995) 182–190.
[81] K. Balasubramanian, Combinatorics of NMR and ESR spectral simulations, J. Chem. Inf. Comput. Sci. 32 (1992) 296–298.